Exploring Motor Imagery-Induced Neural Activation and Corticospinal Excitability in Healthy Adults Using EEG and TMS

by

© Mona Hejazi

A thesis submitted to the School of Graduate Studies
in partial fulfillment of the requirements for the
degree of Master of Engineering.

Department of Electrical & Computer Engineering
Memorial University of Newfoundland

July 2025

St. John's, Newfoundland and Labrador, Canada

I would like to dedicate this thesis to my family.

To my mother, who always encouraged me to strive for the highest goals.

To my sisters, who supported me in all my endeavors.

To my brothers, who taught me the value of hard work.

And to the memory of my father, whom I never had the chance to know, but whose presence I've always felt in my heart.

Abstract

Motor imagery (MI)-based brain-computer interfaces (BCIs) activate motor-related brain regions and, through neurofeedback, foster neuroplasticity, offering significant potential for neurorehabilitation [1]. While MI-BCIs have shown success in restoring hand function after stroke, their use in mitigating upper-limb impairments in multiple sclerosis (MS)—a chronic neurodegenerative disorder characterized by impaired motor control and coordination—remains underexplored [2]. This study presents a preliminary investigation into the feasibility of using MI-BCI for targeted therapy of two specific motor function deficits common in MS: fine motor control and motor coordination. Using two hand tasks representing each of these functions, the objectives were: 1) to examine whether MI of these tasks alters corticospinal excitability (CSE), indicating the potential for fostering neuroplasticity and improving hand function, and 2) to determine if distinct task-specific neural activation patterns can be detected via electroencephalography (EEG), suggesting they may be targeted with BCI-based neurofeedback training.

Data from twenty-one healthy participants (8 males, 13 females; mean age: 41.35 ± 8.36 years) were analyzed for this study. Transcranial magnetic stimulation (TMS) was used to assess changes in CSE due to MI of the coordination and control tasks. A single TMS pulse was delivered during intervals of MI and rest and resulting motor-evoked potentials (MEPs) were measured from the first dorsal interosseous (FDI) muscle. For the control task, MI did not significantly increase MEP amplitudes compared to rest (Δ=39.91 μV, p=.354), but significantly decreased MEP latencies (Δ=−0.34 ms, p=.002). For the coordination task, MI also did not significantly increase MEP amplitudes (Δ= 29.67 μV, p = 0.243), but significantly decreased MEP latencies compared to rest (Δ=−0.30 ms, p = 0.006). CSE was also assessed during actual execution of the tasks (ME), and changes in both MEP amplitudes and latencies were significantly different from rest for both tasks (control: Δ=515.96 μV, $p < .001$; Δ=−1.27 ms, $p < .001$; coordination: Δ=534.98 μV, $p < .001$; Δ=−1.15 ms, $p < .001$).

In a separate session, 64-channel EEG was recorded as participants performed 60 intervals each of MI and ME of the two tasks, as well as rest. To determine if the control and coordination tasks were distinguishable using EEG, several different classification pipelines were explored. In terms of feature extraction, Filter Bank Common Spatial Patterns (FBCSP) based on the five standard EEG frequency bands (delta, theta, alpha, beta, gamma), as well as on a finer set of nine overlapping bands spanning 1–40 Hz in 4 Hz increments, was explored, as were functional connectivity-based features, specifically correlation, coherence, and phase-locking value (PLV). Classification was performed using multiple algorithms, including Linear Discriminant Analysis (LDA), Support Vector Machines (SVM), and Decision Trees (DT). Using the PLV features, classification of control vs. coordination tasks yielded high accuracy (80.5% for MI and 82.7% for ME using a SVM classifier). Accuracies above the chance threshold (i.e., 58.3% for n=120 trials, α=0.05, based on binomial distribution) were obtained for all subjects for both MI and ME, and a majority of participants achieved accuracies above 70%—19 participants for MI and 17 for ME—indicating individual potential for task-specific decoding.

Although MI did not significantly increase MEP amplitude, the consistent latency reductions suggest enhanced corticospinal conduction, likely reflecting subthreshold motor activation. These results may support the potential of MI to facilitate neuroplasticity, despite limited task-specific modulation in excitability. On average, the distinct neural patterns differentiating motor control and coordination were detected with accuracy greater than chance, and for some participants with very high accuracy. Together the EEG and TMS results support the feasibility of targeted BCI-based therapy for improving motor control and coordination. Further work is needed to more reliably and specifically identify the neural activation patterns associated with these functions, particularly in people with MS, and then to evaluate the efficacy of BCI-mediated MI therapy for improving upper limb function in the target population.

Acknowledgements

I would like to express my sincere gratitude to my supervisor, Dr. Sarah D. Power, and co-supervisor, Dr. Michelle Ploughman, for their continuous support, insightful guidance, and encouragement throughout the course of this research. I am truly grateful for the opportunity to have worked with them on this project.

I also extend my thanks to my friends and colleagues at Memorial University of Newfoundland, especially Syed. Z. Raza, for their collaboration, assistance, and support along the way.

I gratefully acknowledge the financial support provided by the Natural Sciences and Engineering Research Council of Canada (NSERC) through the Discovery Grants Program, as well as the endMS Research Studentship funded by the MS Society of Canada.

Finally, and most importantly, I would like to thank my family for their unwavering support and belief in me throughout this journey.

Table of contents

List of tables

List of figures

List of abbreviations

BCI	Brain-Computer Interface
MI	Motor Imagery
ME	Motor Execution
EEG	Electroencephalography
EMG	Electromyography
MS	Multiple Sclerosis
fMRI	Functional Magnetic Resonance Imaging
fNIRS	Functional Near-Infrared Spectroscopy
MEG	Magnetoencephalography
FES	Functional Electrical Stimulation
KVIQ	Kinesthetic and Visual Imagery Questionnaire
CSE	Corticospinal Excitability
MEPs	Motor-Evoked Potentials
FDI	First Dorsal Interosseous
ERD	Event-Related Desynchronization
CSP	Common Spatial Pattern
FBCSP	Filter Bank Common Spatial Pattern
PLV	Phase Locking Value
COH	Coherence
CORR	Correlation
mRMR	Minimum Redundancy Maximum Relevance
SVM	Support Vector Machine
LDA	Linear Discriminant Analysis
DT	Decision Trees
ICEHR	Interdisciplinary Committee for Ethics in Human Research

Chapter 1 Introduction

1.1 Brain-Computer Interfaces (BCIs)

Brain-computer interfaces (BCIs) are transformative technologies that establish a direct communication pathway between the brain and external devices. These systems allow users to control devices such as communication tools, mobility aids, and rehabilitation systems through brain activity alone, thus providing individuals with severe motor disabilities a means to regain lost functions [3]. Users operate BCIs by intentionally generating a set of specific, distinct patterns of brain activity, each associated with predefined device commands. Typically, users generate these patterns by engaging in specific mental tasks. The most common examples are motor imagery (MI) tasks where users imagine movements of body parts like the hands, feet, or tongue, which activates similar brain regions as actual movement [4], [5], [6]. Brain signals are acquired through a functional imaging technology like electroencephalography (EEG), and from them the system interprets the brain activity patterns and translates them into the appropriate device commands [7]. As BCIs have developed, their applications have extended beyond basic communication and control.

1.2. The role of MI-based BCIs in neurorehabilitation

The original motivation behind BCI research was to provide a movement-free means of communication and environmental control for individuals with severe motor impairments [8], [9], [10], [11], that is, to allow these individuals to independently control devices like computers, assistive and augmentative communication devices, and environmental control units. In the past decade, MI-based BCIs have been increasingly explored for use in other applications, including in neurorehabilitation, where they have shown promise in stroke recovery [12]. Strokes often cause damage to cortical areas responsible for motor functions, impairing voluntary movements. If stroke

patients imagine or attempt movement of the impaired limb, MI-BCIs can detect the resulting brain activity from intact motor areas and provide feedback through modalities like virtual reality, functional electrical stimulation (FES), or robotic exoskeletons [13], [14]. This promotes neuroplasticity, the brain's ability to reorganize itself by forming new neural connections in response to learning or injury, thereby strengthening alternative motor pathways to compensate for stroke-damaged areas and aiding in the restoration of voluntary movement [15], [16]. While MI-based BCIs for neurorehabilitation are still under investigation, they offer a promising avenue for restoring motor function after stroke, where they facilitate the engagement of undamaged neural circuits through imagined movements [17], [1], [18], [19], [20].

While MI-based BCIs have demonstrated potential in stroke rehabilitation, their effectiveness in aiding motor function recovery in neurodegenerative diseases like MS remains underexplored. MS is a chronic autoimmune disorder of the central nervous system characterized by myelin degeneration, which disrupts communication between the brain and the body [21]. This results in a wide range of impairments, including fatigue, sensory deficits, cognitive dysfunction, and motor impairments. Despite the significant challenges upper-limb dysfunction, particularly hand impairment, poses to daily activities and quality of life [2], [22], [23], [24], [25]. Motor rehabilitation efforts in MS have largely focused on lower limb function, mobility, and gait, leaving upper-limb rehabilitation underexplored. Given their success in stroke rehabilitation, MI-based BCIs could represent a promising avenue for improving hand function in MS patients by promoting neuroplasticity through targeted neurofeedback [26], [27], [28].

1.3 MI-BCI studies for MS rehabilitation

Several studies have explored the potential of MI, without BCI-mediated sensory feedback, to improve motor performance and enhance upper-limb function in MS by activating neural pathways related to motor control [26], [29], [30], [31], [32], [33]. Although these studies highlighted the promise of MI, their small sample sizes, inconsistent methodologies, and lack of long-term follow-up limited their ability to provide definitive conclusions on its therapeutic potential. Neuroimaging research has provided evidence that MI can activate motor-related brain regions in individuals with MS, supporting its potential role in rehabilitation. However, unlike in healthy individuals and stroke patients, this process is complicated by MS-specific factors such as lesion heterogeneity, chronic demyelination, and neurodegeneration, which disrupt sensorimotor network integrity [34]. The ability of MS patients to perform and process MI tasks may be altered in ways that, for example, require tailored neurofeedback strategies for effective rehabilitation. To date, a very small number of BCI studies have focused on individuals with MS but have shown that MI can be detected via EEG, at least when performing imagery of gross motor skills like clenching the fist, tapping the feet, or walking [35], [36], [37], [38], [39].

Unlike stroke rehabilitation, which primarily targets the restoration of movement that has been suddenly lost, MS often presents unique challenges related to more gradual deficits in fine motor control and coordination [40]. Fine motor control refers to the ability to execute precise, coordinated movements using small muscle groups, particularly in the hands and fingers, which is essential for tasks such as writing or buttoning a shirt. In contrast, motor coordination involves the integration and timing of muscle activation across multiple joints to produce smooth and purposeful movement sequences [41], [42]. In MS, both can be impaired due to damage in key brain regions such as the motor cortex, cerebellum, and basal ganglia, which are essential for these

functions [43], [44]. Additionally, reduced cerebellar grey and white matter volume has been linked to impaired upper-limb coordination [45].

Expanding upon earlier feasibility studies, a recent investigation by Russo et al. [46] demonstrated the feasibility of decoding imagined upper and lower limb movements in individuals with MS using EEG, with classification accuracies exceeding 70% in both movement vs. rest and movement vs. movement conditions. Notably, the study found no significant differences in decodability between limbs with and without weakness or paralysis, underscoring the promise of MI-BCIs even in the presence of motor impairment. These results provide strong support for using MI-based BCIs as a control strategy in MS rehabilitation.

The long term objective of this research is to investigate BCI-mediated MI therapy not just for the restoration of gross motor function, but for the targeted improvement of hand motor coordination and control in individuals with MS. The current thesis research represents a preliminary feasibility study toward this end. In particular, one goal was to gather evidence that MI of tasks representing motor coordination and control would increase corticospinal excitability, which would suggest the potential for fostering neuroplasticity. Another goal was to determine if neural activity related to motor control and motor coordination could be distinguished via EEG, as would be required in a BCI specifically targeting these two functions. As is common in exploratory BCI studies, this preliminary study was conducted with healthy participants in order to establish feasibility and validate methodology prior to engaging the target clinical population of MS patients.

1.4 Research objectives

This preliminary study, conducted with healthy participants, aims to investigate MI tasks targeting motor coordination and control functions. The specific objectives of the study were to:

1. Assess whether MI tasks targeting motor coordination and control can enhance corticospinal excitability, as measured by TMS-electromyography (EMG).
2. Investigate whether EEG can be used to differentiate MI tasks targeting control vs. coordination on a single-trial basis.

By addressing these objectives, the study sought to explore the feasibility of developing MI-based BCIs targeted at improving specific functional deficits like control and coordination, which could be useful in neurodegenerative conditions like MS.

Chapter 2 Literature Review

2.1 Brain-Computer Interface

BCIs enable direct communication between the brain and external devices, bypassing conventional motor pathways. Initially developed to assist individuals with severe disabilities in communication and control; BCIs have evolved into sophisticated systems that offer broader applications [9], [10], [11]. A fundamental aspect of BCI design is MI—the cognitive process of mentally simulating a movement without actual execution. When a user engages in MI, the neural activity in motor-related brain regions, such as the primary motor cortex and supplementary motor area, are modulated in a distinct and detectable manner [5]. BCIs leverage these neural patterns to interpret user intentions and generate corresponding control signals, then translate them into commands for assistive technologies like robotic arms, speech synthesizers, or powered wheelchairs. By enabling interaction with external systems purely through thought, BCIs offer new avenues for restoring lost motor functions and enhancing independence for individuals with physical limitations.

The operation of a BCI follows a structured, multi-stage process that transforms brain activity into executable commands. It begins with the user consciously modulating their brain activity to produce distinct neural patterns associated with specific mental tasks (e.g., imagining left-hand movement vs. right-hand movement). These brain signals are then recorded using non-invasive neuroimaging techniques such as EEG, which measures electrical activity from the scalp. Once acquired, the signals undergo preprocessing to remove noise and artifacts, ensuring data quality. The next step involves feature extraction, where relevant neural characteristics, such as power spectral densities or spatial distributions are identified. The classification algorithm then detects these patterns and associates them with predefined control states. Finally, the extracted information is mapped to control commands, which can be used to operate assistive technologies. This

sequential process enables real-time interaction and adaptation to the user's cognitive input. Figure 2.1 illustrates the main stages of the typical BCI algorithm. A more detailed discussion of these algorithmic stages is provided in Section 2.4.

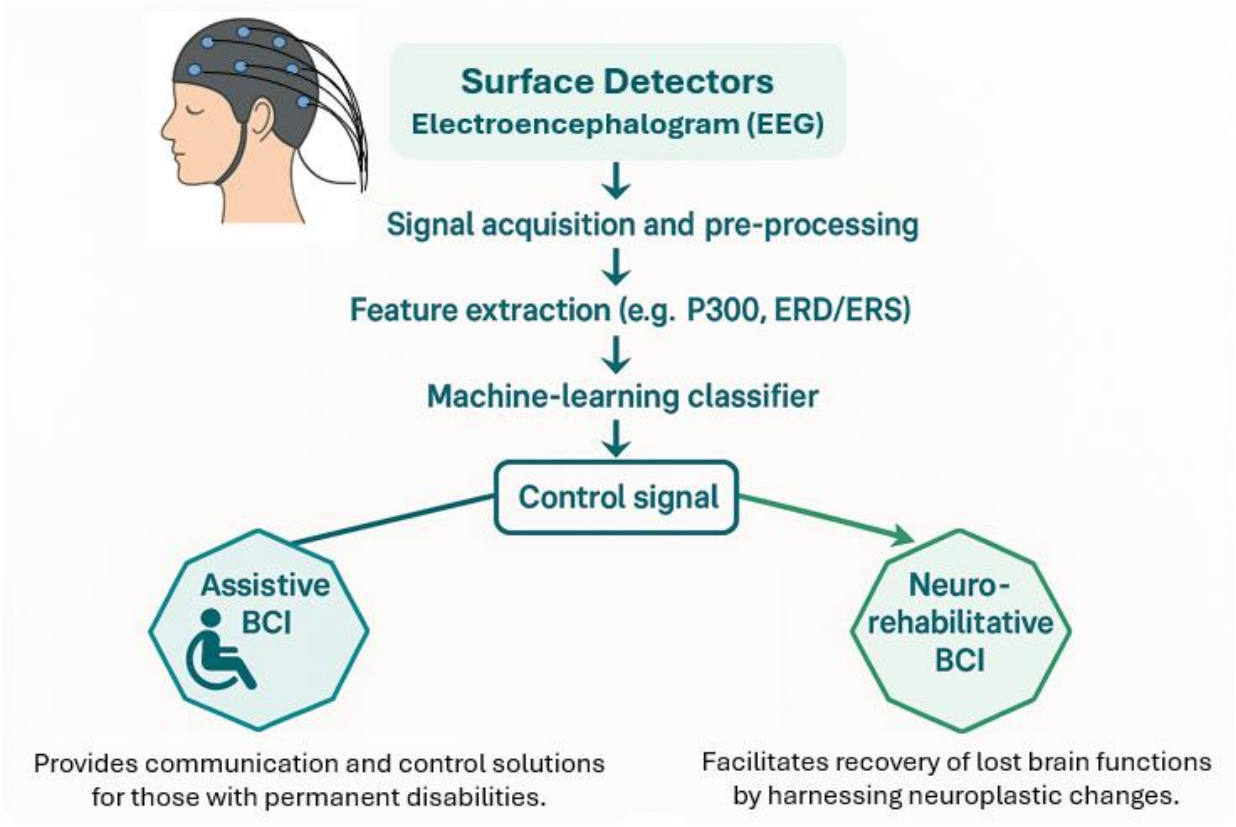

Figure 2. 1. Main stages of the typical BCI algorithm (Image created by the author).

The primary application of BCIs has been to restore communication and control for individuals affected by conditions such as amyotrophic lateral sclerosis (ALS), spinal cord injuries, or stroke, where voluntary motor control is impaired. For individuals with progressive disorders like amyotrophic lateral sclerosis, traditional methods of communication, including speech and gestures, become increasingly ineffective. BCIs offer a solution by allowing users to express intentions and control external devices solely through neural activity. This capability extends

beyond communication, enabling mobility through external devices and facilitating independent interaction with digital interfaces.

In recent years, BCIs have gained significant attention for their potential in neurorehabilitation. MI-based BCIs offer a promising approach to restoring motor function after neurological injuries such as stroke. The brain's remarkable ability to reorganize and form new neural connections is a phenomenon known as neuroplasticity [47]. Unlike passive methods, MI-based BCIs actively engage patients, fostering greater neural reorganization and accelerating motor recovery.

MI-based BCIs deliver real-time neurofeedback through visual, auditory, or proprioceptive cues, guiding users to engage the appropriate neural pathways during imagined or attempted movements. This feedback loop helps reinforce desired brain activity patterns, potentially enhancing the effectiveness of rehabilitation [48]. The integration of BCIs in neurorehabilitation marks a promising expansion of their applications, shifting from purely assistive technologies to tools actively promoting neural recovery. The next section explores the use of MI-based BCIs in neurorehabilitation in greater detail.

2.2 Motor imagery BCIs in neurorehabilitation

2.2.1 Motor Imagery and corticospinal excitability

As previously discussed, MI engages brain regions associated with motor function. Although this activation does not lead to overt movement, it mirrors, at least to some extent, the neural patterns observed during actual motor execution (ME). This similarity in neural engagement is believed to play a role in reinforcing motor-related pathways, thereby supporting motor performance and recovery [49].

MI can be divided into visual and kinesthetic forms. *Visual imagery* involves mentally picturing movements from a first- or third-person perspective, primarily engaging occipital and parietal regions. *Kinesthetic imagery*, on the other hand, focuses on the internal sensation of movement, such as muscle tension and joint position, without actual execution [8]. The Kinesthetic and Visual Imagery Questionnaire (KVIQ) is widely used to assess MI ability, evaluating the clarity of visual images and the intensity of movement sensations on a five-point scale. Both the KVIQ-20 and its shorter version, KVIQ-10, have shown strong reliability and validity in healthy individuals and those with physical impairments, such as stroke patients [50]. The ability to accurately assess MI ability is essential, particularly in neurorehabilitation settings, where MI-based interventions are tailored to enhance motor recovery [51], [52].

Emerging evidence suggests that repeated engagement in MI tasks may enhance corticospinal excitability, hereafter referred to as CSE, which reflects the responsiveness of the corticospinal pathway connecting the motor cortex to spinal motor neurons and may also modulate functional connectivity between motor-related brain regions [53], [54], [55], [56]. These changes have been associated with improvements in motor performance, particularly in the context of rehabilitation following neurological injuries. While the precise mechanisms remain under investigation, MI shows considerable potential as a complementary approach in neurorehabilitation, especially for individuals recovering from stroke, spinal cord injury, or other motor impairments [12].

The integration of EMG with TMS is a common approach for assessing CSE and motor system function [57]. This responsiveness is often evaluated using TMS, which stimulates the motor cortex to elicit MEPs in target muscles [58]. EMG, placed on the muscle corresponding to the brain area being stimulated, records the electrical activity of these muscles, capturing the MEP

responses [59]. This integration provides critical insights into motor pathway integrity, plasticity, and neuromuscular control [60] (see Figure 2.2).

TMS-EMG integration allows for the quantification of key motor system parameters, including MEP amplitude and latency, which serve as indicators of CSE [57]. MEP amplitude, defined as the peak-to-peak voltage of the EMG signal, reflects the excitability of the corticospinal tract, with larger amplitudes suggesting higher CSE and stronger motor pathway engagement. MEP latency, the time delay between TMS stimulation and the muscle response, provides insights into the conduction time of neural signals and synaptic transmission efficiency. These measures are essential for evaluating motor system integrity and detecting abnormalities in neural transmission, making them important tools in both healthy and clinical populations.

TMS-EMG studies strongly support the role of MI in modulating CSE and promoting plasticity within the motor system. Specifically, kinesthetic imagery has been shown to engage the motor cortex in a more effective manner, leading to a greater modulation of CSE compared to visual imagery [61]. Several studies have further elucidated the mechanisms by which MI enhances motor cortex activity and excitability. For instance, Kaneko et al. [62] demonstrated that combining MI with electrical stimulation significantly enhances excitability, reaching levels comparable to voluntary muscle contractions. This finding suggests that voluntary motor drive plays a role in increasing CSE, even in the absence of actual movement. Irie et al. [63] revealed that MI enhances corticospinal transmission via cervical premotoneurons, contributing to oligosynaptic excitation of arm motoneurons. This indicates that MI can effectively activate premotoneuron systems, potentially facilitating motor reacquisition. Furthermore, research by Yoxon and Welsh [64] on cortical plasticity following MI training showed a positive correlation

between the extent of motor system activation during MI and the magnitude of cortical plastic changes. This supports the notion that MI training can drive neuroplastic adaptations, promoting motor learning and functional recovery. Additionally, Foysal and Baker [54] found that delivering TMS during MI selectively enhances motor output in muscles involved in the imagined movement. Collectively, these findings underscore the potential of MI as a valuable tool for motor learning and rehabilitation, particularly when combined with neuromodulatory techniques such as TMS or electrical stimulation.

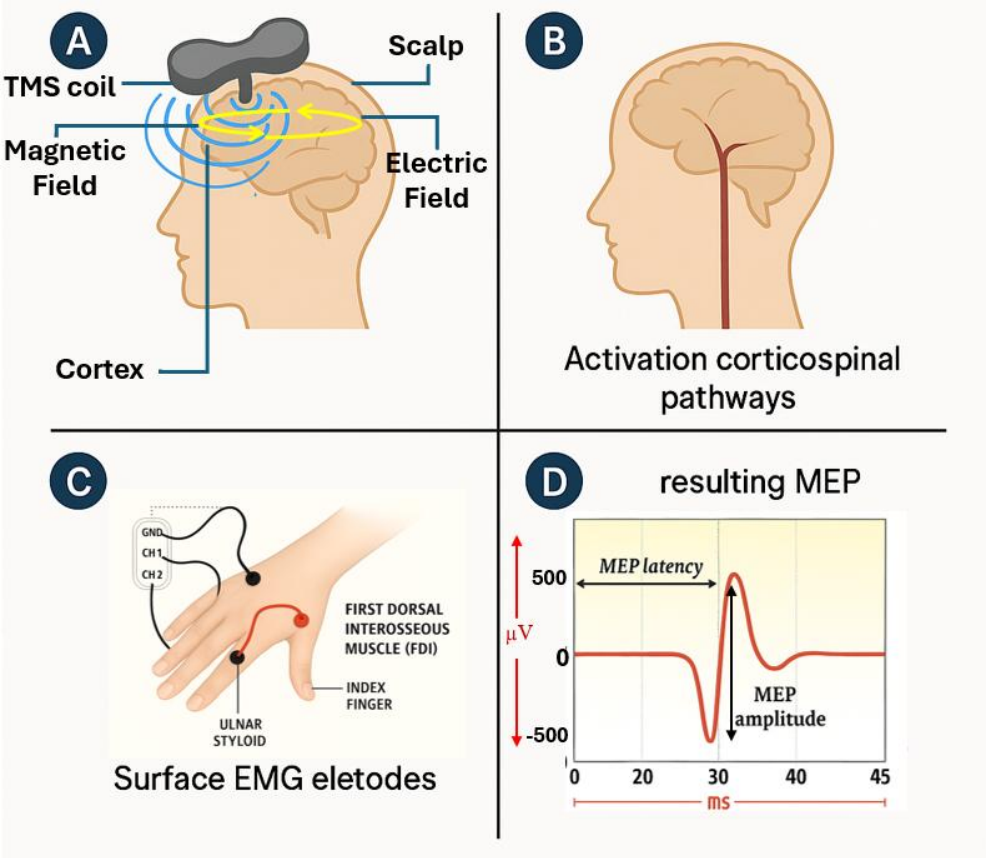

Figure 2. 2. Principles of TMS-induced MEPs: (A) A TMS coil placed over the scalp generates a rapidly changing magnetic field (blue lines), which induces an electric field in the underlying cortex via electromagnetic induction. (B) This non-invasive stimulation activates corticospinal pathways when the coil is positioned over the motor cortex. (C) Surface EMG electrodes are placed on the hand, specifically over the FDI muscle, to record muscle responses. (D) The resulting MEP is characterized by its latency (time from TMS pulse to muscle response) and amplitude (peak-to-peak voltage), which are quantified from the EMG signal. (Image adapted from [65] with modifications by the author.)

2.2.2 Enhancing motor Imagery through neurofeedback in BCIs

The success of MI-based BCIs for neurorehabilitation hinges on neuroplastic mechanisms such as long-term potentiation (LTP), where repeated activation of neural circuits leads to strengthened synaptic connections, in line with Hebbian principles of learning [66]. During MI-based rehabilitation, patients repeatedly activate motor circuits that may have been weakened due to injury or disease, helping to restore lost functions. This process involves both the reactivation of pre-existing neural pathways and the creation of new synaptic connections, leading to motor recovery [67].

MI-based BCIs integrate principles of neurofeedback and closed-loop control systems to further enhance recovery. Through real-time feedback, using neurofeedback mechanisms such as virtual reality, functional electrical stimulation, and robotic exoskeletons, patients can monitor the effect of their imagined movements and adjust their neural commands accordingly [68], [69], [70]. This feedback mechanism facilitates motor learning by reinforcing appropriate neural activation patterns, accelerating motor recovery, and strengthening the association between MI and actual movement. Compared to MI alone, the integration of real-time feedback significantly improves the precision of neural activation, resulting in stronger neuroplastic adaptations and more effective rehabilitation outcomes [71].

2.2.3 Clinical applications of MI-based BCIs in stroke rehabilitation

Numerous studies have demonstrated the effectiveness of MI-based BCIs in enhancing functional recovery post-stroke by engaging lesioned motor pathways and activating intact neural circuits [72]. These systems are particularly promising for upper-limb rehabilitation, where voluntary

control is often compromised. For instance, Ang et al. [13] reviewed three randomized controlled trials involving 67 chronic stroke patients. These trials demonstrated that 26 participants who underwent BCI neurorehabilitation, using strategies such as MI-triggered feedback and robotic-assisted movement, showed significant motor improvement. Specifically, they achieved a mean increase of 4.5 points on the Fugl-Meyer Assessment (FMA) for the upper extremity, highlighting the potential clinical efficacy of BCI-assisted therapy.

Similarly, Ang et al. [14] conducted a clinical study involving 54 hemiparetic stroke patients that assessed the use of EEG-based MI-based BCIs with robotic feedback. Results revealed that 89% of patients could successfully operate the BCI system above the chance level. Participants in both the BCI-robotic and robotic-only rehabilitation groups showed significant improvements in FMA scores post-intervention (mean gains: 4.5 and 6.2, respectively; $p = 0.032, 0.003$) and at 2-month follow-up (mean gains: 5.3 and 7.3, respectively; $p = 0.020, 0.013$), further supporting the efficacy of BCI-based robotic rehabilitation for restoring upper-limb motor function.

In their review article, Khan et al. [1] emphasized the integration of BCI systems with FES, robotic assistance, and hybrid virtual reality models as effective strategies in upper-limb neurorehabilitation. These studies underscore not only the therapeutic potential of these systems but also the need to address technical and clinical challenges. Furthermore, Tong et al. [20] provided neuroimaging evidence showing that MI engages multiple brain areas involved in motor planning and execution, including the cerebellum, basal ganglia, premotor and supplementary motor areas, and the primary motor cortex, suggesting a neural basis for its therapeutic effects.

A meta-analysis by Kruse et al. [73], which included 14 randomized controlled trials involving 362 stroke patients, reported moderate but statistically significant improvements in upper-limb

motor recovery compared to conventional therapy (SMD[1] = 0.39; 95% CI[2]: 0.17–0.62) and enhanced brain function recovery (SMD = 1.11; 95% CI: 0.64–1.59), indicating the effectiveness of BCI-based interventions beyond motor outcomes alone. More recently, Liu et al. [74] re-evaluated systematic reviews and meta-analyses and concluded that BCI training is safe and clinically effective, especially in subacute stroke patients, with positive effects on motor function and quality of life.

In summary, the integration of MI-based BCIs into stroke rehabilitation has proven beneficial in promoting motor function recovery, enhancing neuroplasticity, and supporting the reorganization of neural networks. When combined with neurofeedback, these systems show substantial clinical promise and growing relevance. While MI-based BCIs have been extensively studied in stroke recovery, emerging research is exploring their applicability in other neurological disorders, such as MS, where motor impairments present rehabilitation challenges.

2.3 Potential of MI-based BCI for motor rehabilitation in MS

MI-based BCIs are increasingly being explored as a rehabilitation tool for neurodegenerative conditions like MS, although studies in this area are far less prevalent compared to those focused on stroke rehabilitation.

2.3.1 Multiple Sclerosis

MS is a chronic autoimmune disorder that leads to the degeneration of myelin, the protective sheath surrounding nerve fibers in the central nervous system [21]. This demyelination disrupts nerve

[1] Standardized mean difference (SMD) as a measure of effect size
[2] 95% confidence intervals (CI) as an indicator of the precision of the estimate

signal transmission, causing motor dysfunction, fatigue, and cognitive impairments [75], [76]. As the disease progresses, patients experience increasing difficulty with movement coordination and motor control, often resulting in significant disability.

Rehabilitation strategies for MS typically encompass both unidisciplinary therapies, such as physiotherapy or occupational therapy, and multidisciplinary rehabilitation programs, which involve coordinated interventions delivered by two or more disciplines, including physiotherapy, occupational therapy, speech and language therapy, dietetics, nursing, prosthetics and orthotics, and exercise physiology, often under the supervision of a neurologist or rehabilitation physician [77]. These interventions are administered across various settings, including ambulatory (outpatient/day treatment), home-based, community-based, and inpatient rehabilitation units, providing round-the-clock care [78].

The primary goals are to improve mobility, strength, and daily functioning through physical and occupational therapy, aerobic and resistance exercises, and the use of assistive devices. These conventional approaches aim to leverage neuroplasticity, alleviate symptoms, and sustain functional independence. However, their effectiveness may be constrained by MS-related fatigue, fluctuating disease progression, and individualized treatment responses. Moreover, upper limb dysfunction in MS affects up to 80% of individuals. This remains under-recognized and under-addressed in rehabilitation, despite its substantial impact on independence, daily activities, and the effective use of mobility aids. This gap is partly due to the limited availability and clinical integration of validated performance-based and patient-reported outcome measures tailored for MS [79].

Contrary to strokes, which often results in focal lesions with well-defined recovery trajectories, MS presents a progressive and diffuse pattern of neural damage, requiring a more adaptive and continuous rehabilitation approach [80], [81]. This distinction is important when considering MI-based BCIs for rehabilitation, as MS requires a more dynamic and ongoing approach to support motor function recovery. Emerging evidence indicates that BCI interventions may engage specific neuroplastic processes in individuals with MS. Pinter et al. [82] utilized functional magnetic resonance imaging (fMRI) to assess the impact of EEG-based neurofeedback training in MS patients, finding enhanced fractional anisotropy and increased functional connectivity within key networks such as the salience and sensorimotor systems. These neural changes were associated with improvements in cognitive function, pointing to promising neuroplastic responses induced by BCI use. Such technologies aim to harness the brain's ability to reorganize and adapt. Still, more research is necessary to validate their effectiveness and optimize their integration into MS rehabilitation. The following sections delve into the role of MI in general, followed by a focus on MI-based BCIs and their potential to improve motor outcomes and support sustained recovery in MS.

2.3.2 Motor imagery for rehabilitation in MS

As previously discussed, MI engages brain regions involved in movement and may support neuroplastic changes that contribute to motor recovery in people with MS, as suggested by observed improvements in gait, balance, and fatigue in recent studies [30]. Although it is not yet widely implemented in MS rehabilitation, MI, especially when combined with BCI technology, might offer novel approaches to preserving and potentially enhancing motor function over time.

Several studies have examined MI-based interventions for improving motor function in MS patients. Benito-Villalvilla et al. [30] conducted a systematic review of randomized controlled trials (RCTs) evaluating MI, action observation, and mirror therapy in MS rehabilitation. Their findings revealed that MI, particularly when paired with relaxation techniques or music, significantly improved fatigue, gait, balance, depression, and overall quality of life. Notably, MI combined with music produced greater improvements in gait parameters and quality of life than conventional therapy. Building on these results, Hanson and Concialdi [33] emphasized MI's potential to enhance walking speed and reduce fatigue in individuals with MS. They attributed these improvements to changes in neural networks but also highlighted the need for more rigorous, controlled studies to confirm these effects.

Similarly, Heremans et al. [29] explored how external cues can enhance MI performance in MS patients. Using eye-tracking, they showed that individuals with MS overestimated imagined movement amplitude and exhibited longer eye-movement times compared to healthy controls. Notably, a significant reduction in eye-movement time for MS patients (MS: M[3] = 600 ± 282 ms; controls: M = 284 ± 151 ms) and enhanced spatial accuracy as MS patients showed more accurate eye-movement amplitudes with cues (MS with no cues: M = 227 ± 115; controls with no cues: M = 172 ± 36), suggested that MI may contribute to motor recovery through neural reorganization. However, the addition of visual and auditory cues improved spatial accuracy and shortened MI duration, suggesting that cueing enhances the quality of imagined movements.

In line with this, Seebacher et al. [83] demonstrated the benefits of rhythmic cueing during MI. In their randomized trial, verbally and musically cued MI significantly improved walking speed,

[3] Mean ± standard deviation

walking distance, fatigue, and quality of life. Participants who received rhythmic cueing showed a 25% increase in walking speed and a 30% improvement in walking distance. Additionally, sensorimotor synchronization (SMS) also improved post-intervention, with scores increasing by 18%, indicating enhanced temporal coordination through cueing. The fatigue levels of participants decreased by 22%, and their quality of life scores improved by 15%, further highlighting the positive impact of rhythmic cueing.

Expanding on this line of research, Tacchino et al. [32] further contributed by showing that MI primed ME in MS, suggesting that mental rehearsal can enhance actual motor performance. Participants performed imagined and actual pointing tasks. While healthy controls showed temporal consistency across mental and physical tasks, MS patients exhibited faster imagined than actual movements, particularly with their non-dominant arm. Specifically**,** MS patients showed a significant decrease in execution time for the non-dominant arm in the fifth cycle after MI (from 1.66 ± 0.05s to 1.48 ± 0.06s, $p < 0.05$), whereas healthy controls exhibited no significant differences (1.08 ± 0.04s to 1.05 ± 0.03s, $p < 0.05$), indicating that MI had a greater impact on motor performance in MS patients.

Building on this concept, Lipp et al. [26] provided a conceptual review linking MI to neuroplasticity. They emphasized that motor rehabilitation in MS benefits from the brain's capacity to adapt and highlighted the need for neuroimaging tools to capture MI-driven changes. They argued for MI-based protocols that can modulate plasticity and improve recovery outcomes.

Despite promising results, not all individuals with MS benefit equally. The effectiveness of MI-based rehabilitation may depend on individual factors like disease severity, cognitive function, and baseline MI ability, with some studies indicating that impaired MI ability in MS could limit its

efficacy without additional feedback or adaptive training protocols. For example, Tabrizi et al. [84] provided electrophysiological evidence of MI impairments in MS patients. Using event-related potentials during a mental hand rotation task, they found that MS patients were slower (RT[4] = 1665.95 ± 269.82 ms) and less accurate (83.80 ± 7.72%) than controls (RT = 1505.16 ± 225.11 ms, accuracy = 88.35 ± 7.68%). Neural markers also showed reduced amplitude and delayed latency at P3 in MS patients. These deficits were associated with lower working memory performance, suggesting a cognitive component to MI impairments. Additionally, Tavazzi et al. [27] used neuroimaging to confirm that MI activates motor-related areas in MS patients, offering further validation of its therapeutic value even in the presence of mild disability.

To enhance the effectiveness of MI interventions, there is growing interest in combining MI with real-time BCI feedback. Providing individuals with neurofeedback during imagined movements may help enhance MI engagement, strengthen neural adaptations, and potentially improve rehabilitation outcomes. This approach could address the variability in MI effectiveness across individuals, potentially leading to more consistent benefits.

2.3.3 MI-based BCIs in MS

Emerging research suggests that MI-based BCIs hold significant potential for MS rehabilitation, offering hope for improving gait and restoring motor function. Although BCI applications in MS remain a relatively new and underexplored field, an increasing number of studies have begun to investigate their feasibility (see Table 2.1). For instance, Singh et al. [35] further supported the promise of BCIs to enhance the quality of life in people with MS by reviewing literature across

[4] Reaction time

multiple databases and highlighting BCI as a core technology in future MS rehabilitation strategies, especially in addressing chronic cerebrospinal venous insufficiency and movement impairments.

Building on this, Carolina et al. (Study #1 in Table 2.1) [38] conducted the first study using a BCI coupled with FES for gait rehabilitation in people with MS, including individuals with relapsing-remitting, primary progressive, and secondary progressive forms. Following 24 training sessions over eight weeks, participants demonstrated significant improvements in gait speed ($-1.99\ s$ in the Timed 25-Foot Walk, $p = 0.018$), walking ability (-31.25 points on the MS Walking Scale, $p = 0.028$), and earlier onset of event-related desynchronization (ERD) latency ($-180\ ms$), suggesting a possible enhancement of neuroplasticity.

Additionally, Shiels et al. (Study #2 in Table 2.1) [37] explored the utility of MI-based BCIs for both upper and lower limb tasks in MS. Their findings showed that an MS participant achieved classification accuracies for imagined (0.63 ± 0.01) and executed (0.71 ± 0.04) upper and lower limb movements that were comparable to those of neurotypical participants (imagined: 0.66 ± 0.09; executed: 0.73 ± 0.09), with no significant differences in decoding accuracy or timing, indicating preserved MI signal processing despite the disease.

In [36] (Study #3 in Table 2.1), this same group examined source-level BCI data and found that although the MS participant exhibited substantially reduced alpha power with no clear peak during MI tasks, the identified equivalent current dipoles clustered in both motor cortices alongside those of neurotypical participants. The MS participant's right motor cortex, equivalent current dipole was located 2.13 standard deviations from the control centroid along principal component 3 (Z-score = 1.96, $p = 0.05$), suggesting some spatial separation. Nevertheless, the spectral power

during left- and right-hand imagery tasks remained comparable across hemispheres, with contralateral beta band power reductions of 3.9% in the right motor cortex and 2.6% in the left motor cortex, indicating preserved cortical activation patterns despite the attenuated alpha signal.

In a follow-up study (Study #4 in Table 2.1) [39], they then showed that source-level analysis significantly improved MI classification accuracy compared to scalp-level recordings in both MS and control groups. Importantly, no significant differences were found in classification delays in alpha and beta bands, even for limbs with weakness or paralysis. Notably, source-level classification led to accuracy improvements of up to 7% in individual participants, with average gains of 3% in control participants, 3% in MS participants with affected limbs, and 4% in those without reported symptoms.

These findings underscore the feasibility of MI-based BCI systems for individuals with MS. While most existing research has focused on gait recovery and upper-limb rehabilitation, particularly for improving fine motor function and hand dexterity, the feasibility of MI-based BCI systems remains underexplored. This is significant, as fine motor skills are central to maintaining independence in people with MS. Evidence from stroke and neurorehabilitation studies shows that MI training can enhance grip strength, precision, and coordination by engaging motor cortical areas and supporting neuroplasticity [85]. These improvements are typically measured using standardized tasks like the Nine-Hole Peg Test, which targets functions often compromised in MS [86]. Addressing upper-limb rehabilitation is therefore crucial, as impairments directly impact daily function and overall quality of life. Therefore, targeting control and coordination of the hand through MI-based BCI is not only justified by previous findings in other populations but also aligns directly with the core

objective of this study, which is exploring the feasibility and impact of MI-based BCI for fine motor rehabilitation in MS.

Despite the growing interest in MI-based BCIs for MS rehabilitation, several critical limitations persist in the current body of research:

- **MI tasks:** None of the existing studies defined MI tasks specifically designed to target hand motor control and coordination. Moreover, no studies to date have systematically compared different MI tasks that focus on fine hand movements to determine their relative effectiveness in eliciting distinct and reliable brain responses.
- **Imaging and neurophysiological techniques:** None of the reviewed studies utilized TMS to assess excitability during MI tasks in people with MS. This limits the ability to quantify neurophysiological changes and neural plasticity associated with BCI use.
- **Data analysis techniques:** None of the studies employed FBCSP as a feature extraction method, nor did they evaluate functional connectivity measures during MI as potential features for classification. Furthermore, no study systematically compared multiple classification algorithms within the same dataset to determine optimal decoding strategies in the MS population.

Study #	Author-Year	Objective	# of MS Subjects	Calibration Stage	Feedback Stage	Techniques	Outcomes	Results	Limitations
1	Carrere et al., 2021	BCI-FES for gait rehab	7 (various MS types)	ERD calibration during MI (foot dorsiflexion)	Online: FES triggered by MI detection	EEG (8_{ch}), Laplacian filtering, BCI2000, ERD analysis	Improved gait speed, walking ability, ERD latency	−20.7% T25FW, +46.9% MSWS-12, +15.87% TPR, −180 ms ERD latency	Small sample, no control group, dropouts
2	Shiels et al., 2021	BCI feasibility in MS	1 MS + 7 controls	Executed and imagined clenching (hands) and tapping (feet)	Offline only	EEG (25_{ch}), Wavelet ICA, SVM classification	Comparable MI decoding to healthy controls	>70% accuracy (movement vs rest), No significant difference between executed and imagined tasks	Single MS case, no MS severity evaluation, small sample
3	Russo et al., 2023	Source-level BCI feasibility	1 MS + 7 controls	MI of hand clenching (Go/Stop cues)	Offline only	EEG (24_{ch}), ICA, DIPFIT, clustering	Identified MI-related motor cortical activity	Reduced alpha, preserved beta modulation	Single case, no lesion imaging, no classification
4	Russo et al., 2025	Source-level MI classification in MS	8 MS participants	MI of clenching (hands) and tapping (feet) (Go/Stop cues)	Offline only	EEG (24_{ch}), ICA, DIPFIT, LDA classification	Source analysis boosted classification accuracy	+3–4% accuracy boost, >70% (movement vs rest), ~90% (between movements)	Small sample, age differences, no MRI

Table 2. 1 Summary of MI-based BCI studies in MS (MS: Multiple Sclerosis, Ch: Channels, ERD: Event-Related Desynchronization, T25FW: Timed 25-Foot Walk, MSWS: 12-Item Multiple Sclerosis Walking Scale, TPR: True Positive Rate, ICA: Independent Component Analysis, SVM: Support Vector Machine, DIPFIT: Dipole Fitting, LDA: Linear Discriminant Analysis, MRI: Magnetic Resonance Imaging)

2.4 BCI algorithm

A critical element of BCI systems is the ability to automatically detect different MI patterns from EEG signals. This pattern recognition is essential for interpreting the user's mental state and translating it into meaningful actions. For instance, in communication applications, it may be necessary to differentiate between various MI tasks to issue different commands, such as moving a cursor left, right, up, or down. In rehabilitation scenarios for stroke, the system might only need to detect MI of the affected hand versus rest. In some cases, distinguishing between left and right-hand MI might be beneficial. In studies on gait rehabilitation in MS, researchers typically focused on detecting foot or leg movement versus rest or another similar distinction.

This type of mental state decoding requires sophisticated algorithms capable of interpreting the EEG signals associated with these different MI patterns. As described in Section 2.1, the BCI system involves several stages that work together to process neural signals and translate them into meaningful commands (see Figure 2.3). These stages include: 1) neural data acquisition, 2) signal preprocessing, 3) feature extraction, 4) feature selection, 5) classification, and 6) control with feedback. Each step plays a key role in ensuring the accuracy and efficiency of the system and there are many different options for specific approaches within these stages. Optimizing these stages can significantly improve BCI performance, especially in applications related to rehabilitation and assistive technology, because accurate real-time decoding of MI can directly enhance the user's ability to perform actions or control devices, leading to more effective rehabilitation and greater independence. Feedback is provided during the online usage phase of the system, allowing for real-time interaction and adaptation.

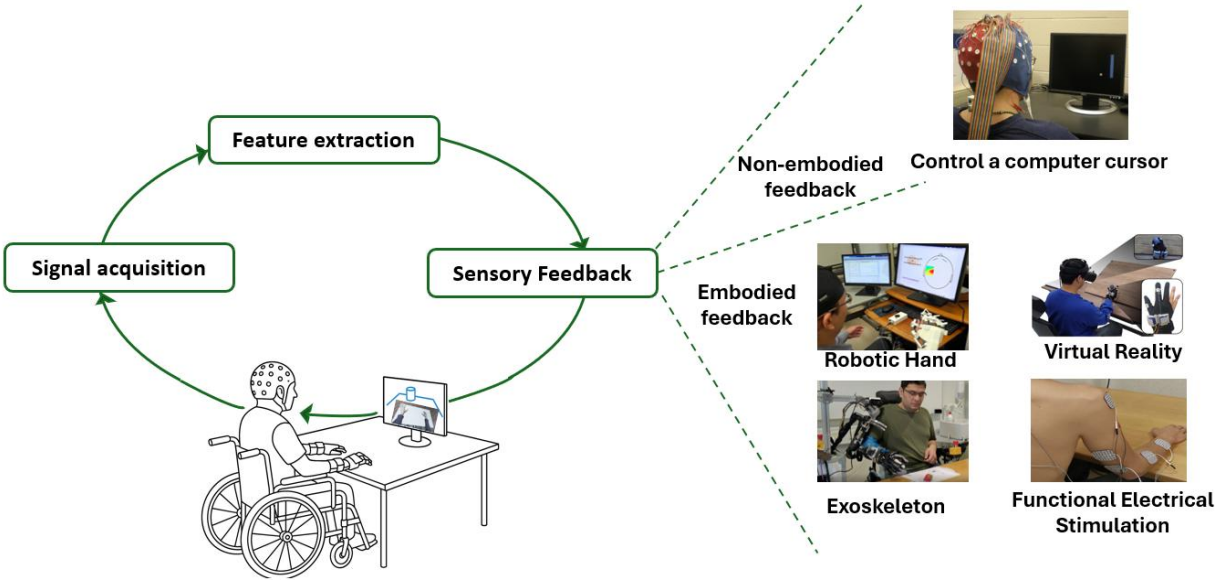

Figure 2. 3. Main stages of the typical active rehabilitative BCI algorithm (Image adapted from [87], [88], [89], [90], [91] with modifications by the author).

2.4.1 Data acquisition

The first step in any BCI system is data acquisition, where sensors capture neural signals as the user interacts with the system. This can be achieved through invasive or non-invasive methods. Invasive techniques involve implanting sensors directly onto or into the brain, offering high spatial resolution and signal-to-noise ratio but posing surgical risks. Non-invasive methods, in contrast, rely on external sensors placed on the scalp, making them more practical for widespread use, though they generally provide lower signal quality compared to invasive techniques [92].

Various recording techniques have been explored in BCI research. Non-invasive methods include EEG [93], magnetoencephalography (MEG) [94], fMRI [95], and functional near-infrared spectroscopy (fNIRS) [96]. Among these, EEG is the most widely used due to its real-time detection capability, portability, and cost-effectiveness [97]. On the other hand, invasive methods such as electrocorticography (ECoG) and intracranial electrode arrays offer higher spatial

resolution and more precise signal capture [98]. However, they are primarily used in clinical research and specialized settings due to their complexity and surgical requirements (see Table 2.2).

The choice of acquisition method depends on the specific application, balancing precision with practicality. EEG is especially popular in neurorehabilitation and assistive technologies due to its relative ease of use in real-world environments, whereas invasive methods are reserved for clinical contexts.

Table 2. 2**.** Commonly used recording methods in BCI systems

Recording Method	**Temporal Resolution**	**Spatial Resolution**	**Cost**	**Portable**	**Invasive**
EEG	High	Low	Low	Yes	No
MEG	High	Relatively High	High	No	No
fMRI	Low	High	High	No	No
fNIRS	Low	Relatively High	Low	Yes	No
ECoG	High	High	High	Yes	Yes
Intracranial Microelectrode Arrays	High	Very High	Very High	Yes	Yes

Electroencephalography

Electrophysiological phenomena

EEG is a non-invasive technique that measures the electrical activity of the brain by detecting the firing patterns of neurons, especially pyramidal cells. These neurons, which are aligned perpendicularly to the cortical surface, generate electrical fields that can be recorded using scalp electrodes. Despite its advantages, EEG has limited spatial resolution, meaning it cannot pinpoint the exact source of brain activity due to signal mixing across different brain regions [99]. However, its high temporal resolution makes it a valuable tool for analyzing rapid changes in brain activity.

EEG data is typically divided into different frequency bands, including delta (1-4 *Hz*), theta (4-8 *Hz*), alpha (8-12 *Hz*), mu (8-12 *Hz*), beta (13-25 *Hz*), and gamma (>25 *Hz*), each associated with various cognitive and motor functions. In MI-based BCIs, imagined movements trigger specific brain activity patterns, such as ERD and event-related synchronization (ERS), particularly within the 7-30 Hz frequency range in the sensorimotor cortex [100], [101].

EEG recording

An EEG recording system consists of three main components: electrodes, an amplifier, and an analog-to-digital (A/D) converter. Electrodes placed on the scalp capture neural signals, which are then amplified to enhance their strength before being digitized for further processing. Given the small amplitude of EEG signals, amplification is necessary to ensure accurate recordings. Conductive gel is often used to reduce impedance, though advancements in dry electrode technology may eliminate this requirement in the future. Figure 2.4 illustrates the EEG recording setup used in this study, incorporating all components discussed above.

The sampling rate of an EEG system, which typically ranges between 128 *Hz* and 512 *Hz*, is chosen to accurately capture the frequency components of neural signals (especially within the 0.5–100 *Hz* range) while minimizing data size and computational load. Additionally, EEG electrodes can be categorized as active or passive. Active electrodes, equipped with pre-amplification circuitry, provide a better signal-to-noise ratio than passive electrodes, making them more suitable for practical BCI systems. Electrode placement follows standardized systems such as the International 10-20 or 10-10 systems [102], ensuring consistent positioning across subjects. Figure 2.5 depicts the standard 10-10 electrode placement system for 64 electrodes.

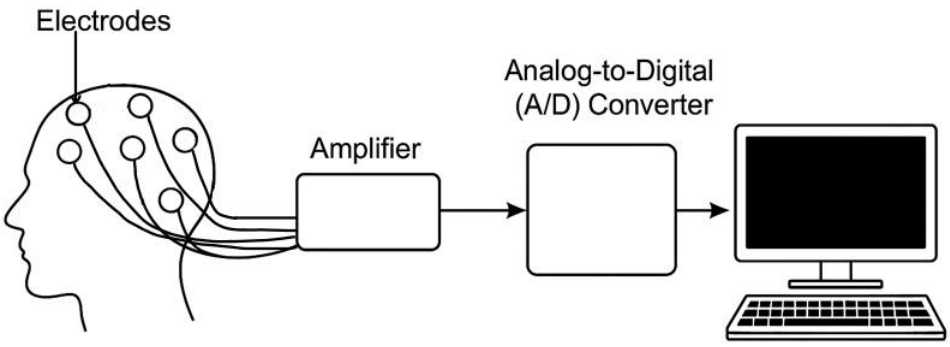

Figure 2. 4. EEG recording setup used in the present study (Image created by the author).

2.4.2 Data preprocessing

Preprocessing is a fundamental step in EEG data analysis, aimed at removing noise and artifacts to enhance the performance of the BCI system. A well-designed preprocessing pipeline ensures cleaner data, improving feature extraction and classification accuracy.

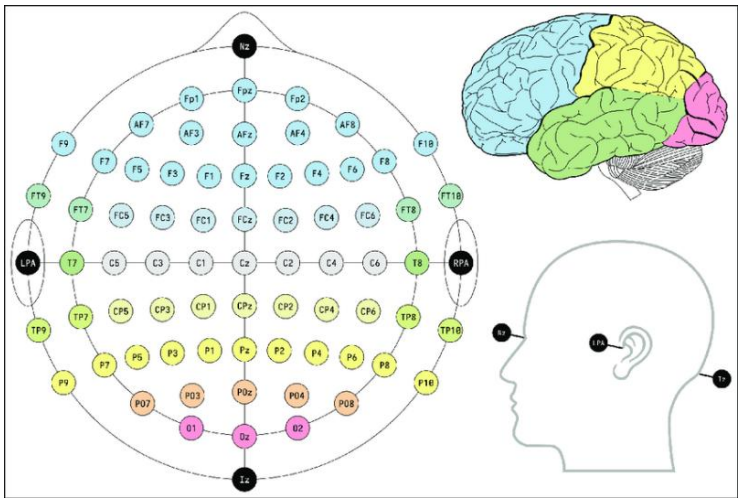

Figure 2. 5. The standard 10-10 electrode placement system (Image adapted from [103]).

Filtering

One of the primary preprocessing techniques is filtering, which isolates relevant frequency components of the EEG signal. Both Finite Impulse Response (FIR) and Infinite Impulse Response (IIR) filters can be used for this purpose. FIR filters are commonly preferred in EEG signal processing because they are inherently stable and provide a linear phase response, which preserves the temporal structure of the signal, crucial for accurate analysis [104]. Typically, a bandpass filter in the range of 1–100 *Hz* is applied to eliminate low-frequency drift and high-frequency noise, ensuring that the desired neural signals are preserved. Often, a notch filter centered at 60 *Hz* is applied to remove power line interference, a common source of electrical noise in EEG recordings.

Re-referencing

During EEG recording, neural activity is captured by measuring voltage differences between each electrode and a designated reference point, which is typically another electrode on the scalp. Re-referencing involves modifying this reference electrode after the data has been recorded. Since this adjustment can influence how the EEG signals are interpreted, it must be applied thoughtfully to maintain data accuracy. One commonly used technique is common average referencing (CAR), where the mean signal across all electrodes is subtracted from each electrode's signal. This method helps reduce common noise and enhances spatial resolution, ultimately improving signal quality and maintaining data integrity [105].

Epoch Extraction

An epoch is a time-segmented portion of EEG data, typically defined around a stimulus or user action. However, in asynchronous BCI systems, epochs can also be extracted continuously,

without being tied to specific task events. Epoching is essential because it structures the EEG data into segments for both training and real-time use. During the training phase, epochs provide labeled samples of distinct mental states, such as rest, MI, or movement, which are used to train classifiers. In the operational (online) phase, consecutive epochs are continuously extracted and classified to decode the user's current mental state and issue appropriate commands in real time.

The length and offset of the epoch play a critical role in capturing relevant neural activity while minimizing artifacts. Choosing the appropriate epoch length is particularly important for different types of tasks or stimuli. For instance, shorter epochs may be ideal for rapid motor tasks, whereas longer epochs might be necessary for cognitive tasks involving sustained attention or memory processing. Careful selection of epoch parameters ensures that the captured data reflects the intended brain activity.

2.4.3 Feature extraction

During the classification phase of a BCI system, the preprocessed EEG data is used to infer which mental task the user is engaged in. Instead of using the raw EEG signals directly, the system typically derives features that reflect representations of the signal that retain the most relevant information for distinguishing between mental tasks. These features often reflect temporal, spatial, and/or spectral properties of the signal. In the time domain, statistical measures like the mean, variance, and standard deviation may be useful for characterizing patterns of neural activity [106]. In the frequency domain, common features include power spectral density and band power, which quantify the signal's power within frequency ranges [107]. To examine how spectral features evolve over time while a task is being performed, time-frequency analysis methods such as the wavelet transform, or short-time Fourier transform can be employed [108].

Common Spatial Pattern (CSP)

CSP filters [109], [110] are a widely used technique in EEG signal processing for extracting relevant features. They are particularly effective for distinguishing patterns of brain activity during MI tasks. The primary goal of CSP is to determine a set of spatial filters that maximize the distinction between two groups of EEG signals (such as MI of left vs. right hand, or MI vs rest). This is achieved by maximizing the signal variance for one group while minimizing it for the other. The CSP features are obtained by applying the spatial filters to the EEG signals and calculating the log variance of the resulting filtered signals. Typically, only the *m* most relevant CSP filters (indicated by the largest eigenvalues) and the resulting features are retained. These features represent the spatial patterns that best distinguish the mental tasks of interest.

Filter bank common spatial pattern (FBCSP)

FBCSP is an extended version of CSP that optimizes spatial filters across multiple frequency bands rather than a single band [111], [112]. This method involves first applying a set of FIR filters to extract signals across various frequency ranges of interest. The CSP algorithm is then applied to each filtered signal, resulting in CSP features being extracted for each frequency band. FBCSP provides a more extensive set of features, offering richer spectral-spatial information, which is often more effective for differentiating between the mental tasks being studied. The features from each frequency band are concatenated into a single feature vector, which is then used for classification or further analysis.

Functional connectivity

Functional connectivity measures interactions between different brain regions, providing insights into neural network dynamics [113], [114]. Several metrics assess functional connectivity, including correlation, coherence, and PLV. These metrics offer complementary views of brain network interactions: correlation evaluates linear relationships between EEG signals, coherence measures frequency-specific connectivity, and PLV quantifies phase synchronization.

Correlation

Correlation evaluates the linear relationship between the activity of two EEG signals over time. A high correlation coefficient (near +1 or -1) indicates that the signals move in a similar (positive) or opposite (negative) direction. In EEG analysis, correlation provides insights into the degree of connectivity between different brain regions by quantifying how strongly their signals are interrelated [115]. Correlation between two signals, ρxy, is calculated as:

$$\rho xy = Cov(x, y) / (\sigma x * \sigma y) \quad (1)$$

where $Cov(x, y)$ is the covariance between the two signals, and σx and σy are the standard deviations of the individual signals.

Coherence

Coherence measures the frequency-specific linear coupling between two EEG signals, assessing the consistency of phase and amplitude relationships within a specific frequency band. Coherence values range from 0 to 1, with higher values reflecting stronger synchronization. This metric is particularly valuable for examining how brain regions interact within distinct frequency bands,

such as alpha, beta, or gamma, during motor tasks [115]. Coherence between two signals is calculated as:

$$Cxy(f) = |Pxy(f)|^2 / (Pxx(f) * Pyy(f)) \quad (2)$$

where $Pxy(f)$ is the cross-power spectral density between the signals, and $Pxx(f)$ and $Pyy(f)$are the power spectral densities of the individual signals.

Phase-locking value

Phase locking value (PLV) quantifies the consistency of phase differences between two EEG signals over time, independent of their amplitude. It focuses on phase synchronization and is useful for assessing the timing of neural interactions. PLVs, ranging from 0 to 1, indicate the strength of phase synchronization, with higher values signifying stronger synchronization between signals. PLV is commonly used to study both transient and long-range connectivity during cognitive and motor processes [115]. PLV for a pair of signals is calculated as:

$$PLV = |(1/N) * \Sigma\, exp(i * (\varphi 1(t) - \varphi 2(t)))| \quad (3)$$

where $\varphi 1(t)$ and $\varphi 2(t)$ are the instantaneous phases of the EEG signals 1 and 2, respectively, at time t, and N is the number of time points.

2.4.4 Feature selection

Feature selection is a critical step in reducing computational complexity and improving classification accuracy. By identifying the most informative features out of the larger pool of features extracted, the system can focus on relevant data while avoiding the inclusion of redundant or irrelevant information that could reduce model performance and increase computational costs.

There are many automatic feature selection algorithms available. One widely used method is the *Minimum Redundancy Maximum Relevance (mRMR)* algorithm [116]. This algorithm is a filter method that, as the name suggests, aims to identify the features that are most relevant to different classes while minimizing redundancy among the features. mRMR measures relevance by evaluating the relationship between each feature and the target class, typically using mutual information or other statistical metrics. Redundancy is assessed by quantifying the pairwise dependencies between features, where high redundancy is indicated by features that provide similar information. In the context of BCIs, mRMR helps ensure that only the most discriminative features are retained, which improves the real-time performance of the system by reducing the computational burden without compromising classification accuracy.

Balancing feature complexity with real-time performance is crucial in BCI systems. While more features may improve classification accuracy, they may also increase the computational burden. Thus, feature selection plays a vital role in ensuring that the BCI system remains efficient and capable of operating in real-time, especially for online applications where low latency is required.

2.4.5 Classification

Machine learning models play a central role in decoding brain activity in BCI applications, particularly in classifying different MI states. In most cases, supervised learning is employed, where the classifier is trained on labeled EEG data, meaning that each training sample is associated with a known task or mental state. During the training phase, the model learns to identify underlying patterns or features in the EEG signals that differentiate between the MI classes (e.g., imagining left-hand vs. right-hand movement). Once trained, the model is evaluated on unseen test data to assess its ability to generalize and accurately classify new brain activity. Popular classifiers

in MI-based BCI systems include LDA, SVM, and Decision Trees, each offering distinct trade-offs in accuracy, interpretability, and computational complexity.

Linear Discriminant Analysis (LDA)

LDA, introduced by Fisher in 1936 [117], finds a linear combination of features that best separates two or more classes by maximizing inter-class variance and minimizing intra-class variance [118]. This projection onto a lower-dimensional space makes it efficient for high-dimensional data, particularly when there are more samples than features. Its speed and simplicity make LDA a strong candidate for real-time BCI applications. However, LDA assumes normally distributed data with equal class covariances, which may not always hold in EEG data [119]. It is also sensitive to outliers and limited in handling nonlinear relationships. Regularized Linear Discriminant Analysis (RLDA) [120] addresses overfitting by introducing a bias-adjusting hyperparameter. Despite its limitations, LDA remains one of the most widely used classifiers in MI-based BCI systems due to its efficiency and strong real-time performance [121].

Support Vector Machines (SVMs)

Introduced by Cortes and Vapnik in 1995 [122], SVMs solve binary classification tasks by constructing a hyperplane that maximizes the margin between classes. This approach ensures good generalization, particularly for high-dimensional and complex datasets like EEG signals. SVMs handle non-linear data through the “kernel trick”, which implicitly maps inputs into a higher-dimensional space using kernel functions such as polynomial or radial basis functions. For non-separable data, the “soft margin” method introduces slack variables and a regularization parameter (C) to balance training accuracy and model complexity. SVMs are among the most widely used classifiers in MI-based BCI systems due to their robustness, high classification accuracy, and suitability for complex EEG data. They have demonstrated superior performance in numerous

studies, including those by Wu et al. [123] and Ghane et al. [124], who showed that SVMs outperform many alternative classifiers in distinguishing between different MI tasks. As reviewed by Cao [125], SVMs are particularly effective in handling noisy or outlier-contaminated EEG features through regularization, managing high-dimensional data without significant performance loss, and maintaining stability in the presence of non-stationary signal patterns. These strengths have made SVMs a reliable choice for both offline analysis and real-time BCI applications, where accuracy and generalizability are essential.

Decision Tree (DT)

Decision Trees classify data by recursively splitting the feature space based on decision thresholds, resulting in a tree structure of conditional rules [126]. Their interpretability makes them valuable in clinical and research applications, where understanding decision logic is crucial. In the context of MI-based BCIs, Decision Trees are not typically the top-performing standalone classifiers due to their tendency to overfit noisy, high-dimensional EEG data. However, pruning techniques and ensemble methods (such as Random Forests and Boosted Trees) can help improve generalization and stability by reducing overfitting and enhancing robustness. While Decision Trees are not always the top choice for final classification in MI-based BCIs, they are valuable for feature selection and often serve as components in ensemble pipelines. Recent work by Guan et al. [127] introduced a subject-specific decision tree (SSDT) framework combined with Riemannian geometry to classify MI EEG signals, demonstrating improved recognition rates across multiple datasets. These findings underscore the potential of Decision Tree-based approaches when integrated into more sophisticated classification frameworks.

Computational Trade-offs

Each classifier offers a unique balance between accuracy, interpretability, and efficiency. LDA is fast, effective, and remains a standard in real-time applications, though limited in modeling complex, non-linear EEG data [128]. SVMs offer greater flexibility and often yield higher classification accuracy in offline settings, particularly when using non-linear kernels. However, in the linear case, which is commonly employed in MI-BCIs, SVMs maintain comparable efficiency to LDA, making them suitable for real-time use with minimal optimization [121]. Decision Trees are interpretable and fast at inference but can overfit and exhibit high variance. More advanced methods, such as ensemble models, Riemannian geometry-based classifiers, tensor decomposition, and deep learning, offer improved accuracy and robustness but often require large datasets, extensive calibration, and significant computational resources. Adaptive and transfer learning approaches show potential for addressing EEG variability (e.g., across participants and across sessions), though their real-time viability is still under evaluation [129]. Ultimately, while newer methods offer promise, LDA and similarly efficient models remain competitive for real-time MI-based BCI systems due to their simplicity, speed, and robustness.

2.4.6 Feedback / Control

The effectiveness of MI-based BCIs can be significantly enhanced through real-time feedback and control mechanisms. Feedback serves as a crucial component in training users, reinforcing learned MI strategies, and improving overall performance, which refers to the system's ability to accurately detect and classify MI-related brain activity, as well as the user's ability to modulate their mental states effectively to achieve desired control outcomes. Various feedback modalities have been explored, including visual feedback, which provides real-time graphical representations such as

cursor movements or virtual reality simulations [130]; auditory feedback, where sound cues like pitch variations or synthesized speech guide users, especially those with visual impairments [131]; haptic feedback, delivered through vibrations or wearable actuators to reinforce correct MI execution, particularly in rehabilitation settings [132]; and, robotic feedback, where robotic devices or exoskeletons offer physical movement responses to MI-based control signals, aiding neurorehabilitation and assisting individuals with motor impairments in regaining movement functions [133].

In terms of online BCI use, feedback has a critical role in reinforcing correct brain activity patterns in real time. Adaptive feedback systems, which dynamically adjust based on the user's performance, are particularly valuable in BCI rehabilitation [134]. These systems can enhance motor learning by providing timely cues that guide the user toward optimal MI strategies, improving both engagement and task performance.

2.4.7 BCI Performance Evaluation

In real-world BCI applications, classification typically occurs online, meaning the system must interpret and respond to new EEG data in real time. The performance of such systems is evaluated based on how accurately they can classify unseen brain signals as the user engages in tasks like MI. However, many exploratory or early-stage BCI studies assess classifier performance offline, that is, using data that has already been fully collected prior to classification. This allows researchers to experiment with different algorithms and parameters before deploying a real-time system. In offline evaluation, the available dataset must be split into training and testing sets. A simple approach involves a single split, such as an 80% training and 20% testing division.

However, this method can produce performance estimates that depend heavily on which data samples are included in each set.

To obtain a more reliable and unbiased estimate of classifier performance, researchers often use *K-fold cross-validation (CV)* [135]. In this method, the dataset is divided into K equally sized subsets or folds. For each of K iterations, the model is trained on K−1 folds and tested on the remaining fold. This process ensures that each data point is used for both training and testing exactly once. The classifier's accuracy, defined as the percentage of correctly classified samples out of all test samples, is computed for each fold, and the final performance is reported as the average accuracy across all K folds. K-fold CV reduces the likelihood of overfitting to a particular training subset and provides a more generalizable performance estimate. Additionally, performance evaluation may also involve other metrics such as precision, recall, F1-score, and confusion matrices, particularly in multi-class classification problems or imbalanced datasets. These metrics help assess not just overall accuracy but also how well the model differentiates between specific MI classes.

Chapter 3 Methods

3.1 Participants

Twenty-nine healthy participants were recruited for this study. Recruitment materials were distributed through social media platforms (Facebook, Twitter, Instagram, etc.), posters, and Memorial University's official weekly internal email bulletin that was sent to all faculty, staff, and students. Eligibility was confirmed through a pre-screening phone call before participation. Participants were eligible if they were aged between 30 and 60 years, right-handed (as confirmed by the Edinburgh Handedness Inventory), had normal or corrected-to-normal vision and hearing, had no history of seizures or epilepsy, head trauma, primary psychiatric disorders, neurodegenerative diseases, or manual dexterity impairments, were not taking medications contraindicated for TMS, had not previously experienced adverse reactions to MRI or TMS, and did not have any other TMS contraindications as determined by responding "no" to all ten questions in Table 3. Participants were instructed to refrain from exercising, consuming alcohol or caffeine for at least four hours, and using cannabis for 24 hours prior to the experiment. At the beginning of the first session, all eligibility criteria were reconfirmed.

Table 3. 1. TMS screening form

1.	Do you have epilepsy, or have you ever had a convulsion or a seizure?
2.	Have you ever had a fainting spell or syncope (loss of consciousness)? If yes, please describe on which occasion:
3.	Have you ever had a head trauma that was diagnosed as a concussion or was associated with a loss of consciousness?
4.	Do you have any hearing problems or ringing in your ears?
5.	Do you have cochlear implants?
6.	Are you pregnant or is there any chance you might be?
7.	Do you have metal in the brain, skull, or elsewhere in your body (e.g., splinters, fragments, clips, etc.)?
8.	Do you have an implanted neurostimulator (e.g., DBS, epidural/subdural, VNS)?
9.	Do you have a cardiac pacemaker or intracardiac lines?
10.	Do you have a medication infusion device?

Informed written consent was obtained from all participants before the first experimental session. The study was approved by the Interdisciplinary Committee on Ethics in Human Research at Memorial University of Newfoundland (ICEHR#:20222170). Data from twenty-one participants (8 males, 13 females; mean age: 41.35 ± 8.36 years) were included in the final analysis. Eight participants had to be excluded due to incomplete or low quality data.

3.2 Instrumentation

3.2.1 TMS and EMG

TMS was administered using a Magstim BiStim 200^2 magnetic stimulator (Magstim Co., Whitland, UK) connected to a double 70 mm figure-of-eight coil (Magstim, Co.). The TMS pulses were monophasic and delivered over the hand area of the primary motor cortex. During all procedures, the TMS coil was held tangentially to the scalp with the handle pointing backward and laterally at an angle of 45^{o} from the midline and perpendicular to the central sulcus (As illustrated previously in Figure 2.2. A). This position delivers posterior-to-anterior directed TMS pulses that produce large MEPs resulting from the gradual recruitment of I-waves [136].

Neuronavigation was performed using Brainsight™ (Rogue Research, Montreal, QC, Canada) guided the TMS coil position. Brainsight™ was also used to sample and store MEPs with its built-in EMG system. The built-in EMG system in Brainsight™ employed a total amplification of 2500 *V/V*, with a primary amplifier gain set to 600 *V/V*. Signals were sampled at 3 *kHz* and filtered within a bandwidth of 16–550 *Hz*. The Montreal Neurological Institute (MNI) brain template was rendered within the Brainsight™ software and used as a 3D stereotaxic reference to guide the coil positioning [137]. EMG data were recorded at a 3 *kHz* sampling rate using Brainsight™ EMG software, with each trial consisting of a 900 *ms* sweep (100 *ms* pre-stimulus and 800 *ms* post-

stimulus). To prevent overheating, the TMS unit was positioned near an air conditioner, and the coil was rested on a cooling pad between trials when necessary.

3.2.2 EEG

EEG data were recorded using a 64-channel actiCHamp system with actiCAP electrodes (Brain Products GmbH), sampled at 500 Hz. The impedance of all electrodes was kept below 10 $KOhm$ Sampling frequency throughout the experimental session to ensure high-quality signal acquisition. Electrodes were placed according to the International 10-10 system.

3.3 Experimental protocol

Motor imagery and execution tasks

MS patients often experience impairments in fine motor coordination and control due to deficits in corticospinal and sensorimotor integration [138]. Thus, this study examined two right-hand tasks designed to represent these distinct aspects of motor function: motor coordination and motor control. The *motor coordination task* involved sequentially touching each fingertip to the thumb at the participant's own pace and repeating the sequence throughout the task interval (see Figure 3.1a) [42]. This task was selected because it requires precise timing, sequencing, and smooth transitions between discrete movements, which are key elements of motor coordination. In contrast, the *motor control task* required repeated cycles of full hand extension followed by bringing the thumb and fingertips together while maintaining straight fingers and thumb without flexion at the finger joints (see Figure 3.1b) [41]. This task was chosen to emphasize fine motor control, as it demands sustained, precise regulation of muscle activation to maintain joint positions and suppress unintended flexion.

Participants performed both MI and ME of these tasks, resulting in four conditions: 1) $Control_{ME}$ (execution of the control task), 2) $Control_{MI}$ (imagery of the control task), 3) $Coordination_{ME}$ (execution of the coordination task), and 4) $Coordination_{MI}$ (imagery of the coordination task). Additionally, a Rest condition was incorporated, in which participants were instructed to keep their eyes open and focus on the screen (they could blink normally) and refrain from executing or imagining any movements. During the MI trials, they focused on the kinesthetic experience of the imagined actions [139].

a) Motor Coordination b) Motor Control

Figure 3. 1. Visual representation of the two motor tasks performed under MI and ME conditions: a) Motor Coordination and b) Motor Control (Image created by the author).

3.3.1 Session #1: TMS

Before the TMS procedure, participants completed a TMS safety screening and provided informed consent. Following this, the KVIQ-10 [50] was administered to assess their MI ability and help them understand the difference between kinesthetic and visual MI.

Calibration

The TMS experiment began with the system's calibration. Using the Brainsight™ neuronavigation software, we first established the spatial positioning of both the coil and the participant's head in three dimensions with the aid of an infrared camera and a template brain image. The coil, equipped with infrared markers, was calibrated using a standard coil calibration plate. The participant was

seated in a custom-designed chair featuring a headrest and armrests. To facilitate precise anatomical identification, the participant wore infrared marker-equipped glasses, and a similarly equipped pointer was used to mark key anatomical landmarks, including the nasion and the left and right tragus of the ears. Throughout the TMS procedure, the participant continued wearing the infrared glasses to ensure accurate tracking of the coil and stimulus location. Next, the participant's right hand was prepared for EMG electrode placement. Three specific areas were prepared: the first dorsal interosseous (FDI) muscle, the index finger, and the ulna styloid process (see Figure 3.1D). Preparation included shaving the area (if necessary), gentle abrasion with scrubbing gel, and cleansing with 70% isopropyl alcohol wipes to minimize electrical resistance and optimize signal quality.

Motor hotspot identification

The motor hotspot is the specific cortical site within the motor map that elicits the largest and most consistent MEPs in response to TMS. It represents the optimal stimulation point for activating a targeted muscle, in this case, the FDI muscle. Motor mapping techniques provide a reliable method for identifying the motor hotspot, minimizing variability and inter-experimenter subjectivity.

To locate the hotspot, a magnetic stimulator connected to a double figure-of-eight coil was used. The coil was positioned tangentially to the scalp with the handle oriented 45° posterior-lateral from the midline, ensuring a posterior-to-anterior current flow in the motor cortex. A 6 $cm \times 7\ cm$ virtual grid was overlaid on the primary motor cortex corresponding to the contralateral hand area, as guided by neuronavigation software. The coil was systematically moved across the grid, and suprathreshold TMS pulses (capable of eliciting ~500 μV MEPs) were delivered to each grid point

at random inter-trial intervals (between 3–5 s). The hotspot was defined as the location where the largest, most consistent peak-to-peak MEP was recorded in the FDI muscle.

Determination of resting motor threshold (RMT) and experimental stimulus intensity

The resting motor threshold (RMT) is defined as the minimum TMS intensity (% of maximal stimulator output, MSO) required to elicit an MEP of at least 50 μV in five out of ten consecutive trials while the participant maintains complete muscle relaxation. RMT serves as an index of excitability at rest and is a key parameter for determining stimulation intensity in TMS studies.

To ensure accurate RMT measurement, participants sat comfortably with forearms resting on a pillow to minimize muscle tension, while surface EMG electrodes monitored background activity. If excessive EMG was detected, they were instructed to relax fully or perform a brief maximal voluntary contraction followed by relaxation. Once RMT was established, the TMS stimulus intensity for the main experiment was set at 120% of RMT (1.2 × RMT as % MSO) to ensure consistent cortical activation across participants.

Experimental protocol

Before beginning the experiment, participants received a tutorial and explanation of the task requirements in the TMS room, immediately after determining their RMT and motor hotspot. They were guided through the experimental procedures, familiarized with task cues, and allowed to complete practice blocks to ensure they fully understood the instructions. The experiment was designed using PsychToolbox in MATLAB and consisted of alternating Task and Rest blocks, totaling five Rest blocks and four Task blocks. Figure 3.2 illustrates the details of each block.

Task blocks: Each task block consisted of five runs, with each run containing four trials—one for each of the four task conditions: $Control_{MI}$, $Coordination_{MI}$, $Control_{ME,}$ and $Coordination_{ME}$. The task order was randomized within each block. Each trial lasted 8 seconds, with TMS pulses automatically delivered at 2 and 7 seconds. An 8-second rest period, free of TMS stimulation, separated consecutive trials. Transitions between task and rest were indicated by visual cues on the computer screen. The total duration of each run was 64 seconds.

Rest blocks: Rest blocks were used to get a baseline measure against which to assess the effects of MI and ME on excitability. The rest blocks were thus designed to be as similar as possible to the Task blocks. Each Rest block contained one run, consisting of four Rest trials. Like Task trials, each Rest trial lasted 8 seconds, with TMS pulses automatically delivered at 2 and 7 seconds. An 8-second rest period, free of TMS stimulation, separated by consecutive Rest trials. No cues were given to distinguish between Rest trials (with pulses) and rest intervals (without pulses). The total duration of each run was 64 seconds.

In total, 20 trials of each of the five conditions ($Control_{MI}$, $Coordination_{MI}$, $Control_{ME}$, $Coordination_{ME,}$ and Rest) were completed, with 40 TMS pulses administered per condition. At least three-minute breaks were provided after each block, allowing participants to rest and refocus before continuing the experiment. At the conclusion of the session, the experimenter removed the infrared glasses and adhesive EMG electrodes from the participant's hand.

Initially, we considered using Rest trials within Task blocks (intermixed with task trials) as a baseline. However, we found that these intervals were influenced by the preceding task, as the brain does not transition instantly between active and resting states. This carryover effect altered the MEPs recorded during these rest periods, making them unreliable for baseline measurements.

To achieve a more stable and accurate baseline, we instead implemented dedicated Rest blocks, where isolated rest trials with TMS pulses provided more consistent and reliable results.

The automatic TMS triggering system was implemented by establishing a connection between the PsychToolbox script, the parallel port, and the TMS stimulator. PsychToolbox, running on MATLAB, controlled the timing of stimulus presentation and generated digital output triggers via the computer's parallel port. These triggers were sent to the TMS device, ensuring precise stimulation at predefined task events. To facilitate synchronization, a parallel port interface was configured to transmit TTL pulses, which were detected by both the TMS stimulator and the EMG recording system. The EMG system captured the incoming triggers alongside the muscle activity data, allowing for accurate temporal alignment of TMS pulses with motor responses. Additionally, a specific delay was accounted for in the script to correct for hardware latency, ensuring that the stimulation coincided precisely with the intended cue. This setup enabled a seamless and automated synchronization of TMS pulses with experimental events, improving the reliability of motor response measurements.

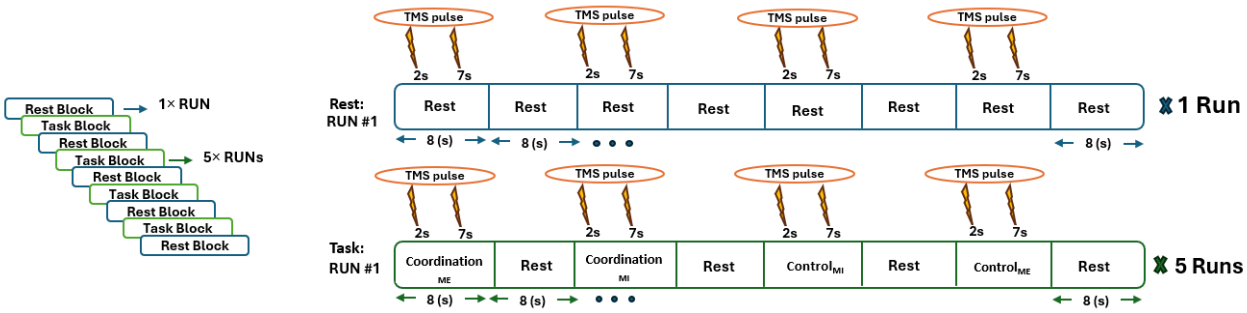

Figure 3. 2. The TMS experimental protocol included five rest blocks and four task blocks. Rest blocks included trials of rest, with participants receiving two pulses per trial. Task blocks involved imagining or executing coordination or control tasks, with two TMS pulses administered per trial. By the end of the session, 20 rest trials (40 TMS pulses) and 20 task trials (40 TMS pulses) per condition were completed for each task (Image created by the author).

3.3.2 Session #2: EEG protocol

The second session took place within the same month as the first. Participants were seated comfortably, and a flexible cap with 64 electrodes was placed on their head and secured with a Velcro strap under the chin. Electrolyte gel was applied to each electrode to ensure optimal connection between the electrodes and the scalp. EEG signals were recorded while participants engaged in tasks consistent with those from the TMS/EMG session, with additional trials to enhance classification accuracy. Two baseline trials of 60 seconds duration, one with eyes open and one with eyes closed, were collected prior to the start of the main part of the experiment.

Participants completed six blocks, each consisting of 10 runs. Each run included five trials for each of the five conditions: $\text{Control}_{\text{ME}}$, $\text{Coordination}_{\text{ME}}$, $\text{Control}_{\text{MI}}$, $\text{Coordination}_{\text{MI}}$, and Rest. The task order was random within each block. Participants took a three-minute break between blocks.

Prior to the start of each trial, the task the participant was to perform (or rest) was indicated by a visual cue on the screen. Participants initiated each trial when ready by pressing the space key. Following the key press, a fixation cross was displayed for 2 seconds, followed by a 4-second blank screen during which participants either performed a task or rested as appropriate, followed by the fixation cross for another 2 seconds to end the trial. Each trial was thus 8 seconds in total. To synchronize EEG data with the cues, an event marker was sent from PsychToolbox to BrainVision Recorder at the beginning of each trial. This ensured precise alignment between the recorded EEG signals and the experimental events, allowing for accurate segmentation and analysis. The experimental protocol, including trial timing, is summarized in Figure 3.3. In total, participants completed 60 trials for each of the five conditions (6 blocks × 10 runs × 1 trial per run). After completing all blocks, two additional baseline trials of 60 seconds duration, one with

eyes open and one with eyes closed, were collected. At the conclusion of the session, the experimenter removed the cap from the participant's head, and any excess gel was easily removed with water and shampoo.

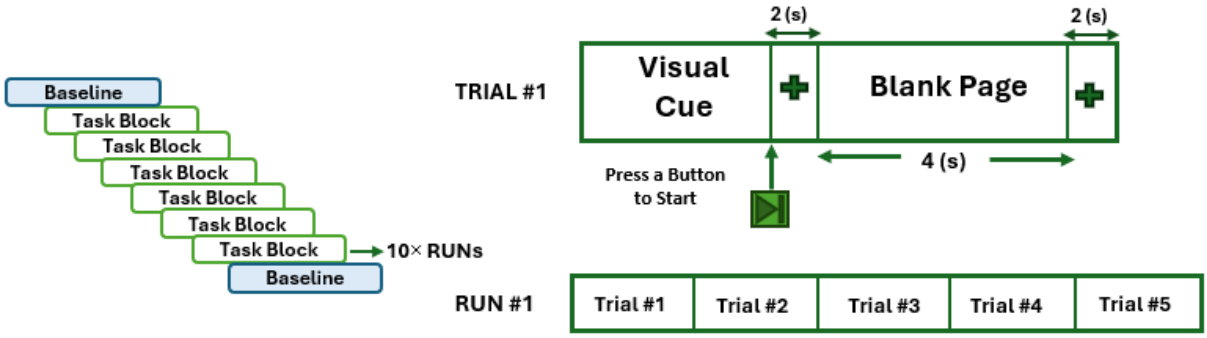

Figure 3. 3. The EEG experimental protocol involved trials initiated by a visual cue, followed by a 2-second fixation cross and a 4-second blank screen during which participants performed one of the five conditions. Each trial ended with another 2-second fixation cross. Participants completed 60 trials for each of the five conditions (6 blocks × 10 runs × 1 trial per run) (Image created by the author).

3.4 Data analysis

3.4.1 TMS/EMG data: extracting MEP amplitudes and latencies

The amplitude and latency of the MEPs induced by TMS pulses were used as measures of excitability. MEP amplitude was defined as the peak-to-peak voltage of evoked EMG response, calculated as the difference between the maximum positive and negative deflections within a fixed 50 *ms* post-stimulus window following the TMS pulse. This measure reflects the responsiveness of the corticospinal pathway, with larger amplitudes indicating greater excitability (see Figure 3.4).

MEP latency was identified by the time point when the EMG signal first exceeded a threshold set at three times the standard deviation above the mean of the background EMG in the 50 ms window preceding the TMS pulse. This latency represents the conduction time from the motor cortex to

the target muscle, providing insights into neural transmission speed and integrity. To extract MEP amplitude and latency from the EMG signals, a structured pipeline was followed.

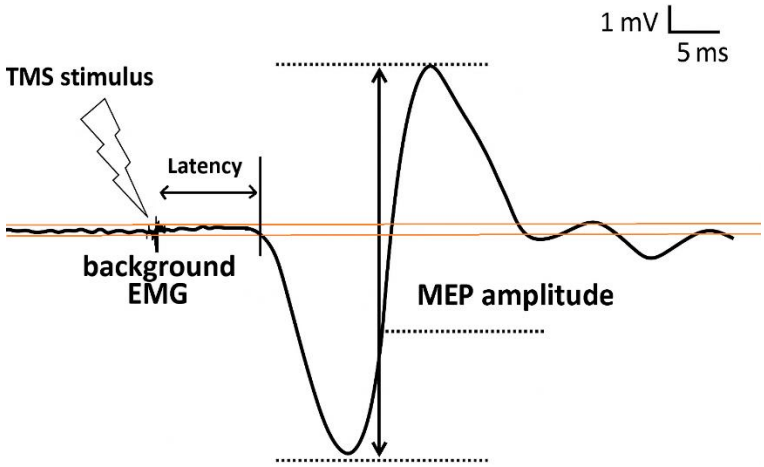

Figure 3. 4. MEP Characteristics: MEPs are elicited by TMS stimulation and recorded via EMG. MEP amplitude is the peak-to-peak voltage of the response, while MEP latency is the time from the TMS pulse to the first detectable response exceeding baseline background EMG noise (Image created by the author).

Trial inclusion and exclusion criteria

Automatic and manual detection of MEP features

A MATLAB script was developed to automatically extract MEP features, including onset latency and amplitude, based on an algorithm adapted from a previously established method [4]. The script processed EMG recordings from multiple participants across several trials to quantify the neural response to each TMS pulse. Each trial contained two TMS pulses, and each condition included 20 trials, resulting in a maximum of 40 MEPs per condition. The automatic algorithm followed a systematic approach:

1. **Data loading and segmentation**: For each subject, EMG data were loaded and segmented into fixed-length sweeps of 900 *ms* per trial, sampled at 3 *kHz* (thus totaling 2700 data

points per trial). The first 300 samples (i.e., the initial 100 *ms*) were used to estimate the background EMG, while the subsequent samples (post-TMS) contained the MEP response.

2. **MEP onset detection**: A dynamic threshold was calculated as three times the standard deviation plus the mean of the background EMG. The MEP onset was defined as the first point in the response window (typically 15–50 *ms* post-stimulus) that exceeded this threshold and was followed by two consecutive increases in absolute amplitude, to reduce false detections due to noise. If no such pattern was found, the trial was considered a non-response.
3. **MEP latency calculation**: For valid MEPs, latency was computed as the time (in milliseconds) from the TMS pulse to the detected onset sample, adjusted by the sampling rate (3 *kHz*).
4. **MEP amplitude calculation**: Within the post-onset MEP window, the positive and negative peaks were identified using the *findpeaks* function. The MEP amplitude was computed as the sum of the absolute values of the maximum positive and minimum negative peak amplitudes (i.e., peak-to-peak amplitude).
5. **Handling missing data**: If no valid MEP was detected, latency and amplitude were assigned *NaN* values, and the trial was flagged for exclusion from further statistical analyses.

Manual review and trial exclusion

While the automatic MEP detection algorithm was able to identify most MEPs and correctly calculate the amplitude and latency, it was not 100% accurate. The primary reasons for failure included:

- Low signal-to-noise ratio, leading to difficulty in detecting clear peaks.
- Overlapping muscle activity masking the MEP response.
- Inconsistent background EMG, affecting threshold determination.

The automatic latency extraction algorithm failed in 21.25% of pulses during task conditions and 16.25% of pulses during rest conditions. Considering the number of pulses per condition (160 for task and 40 for rest), the overall failure rate across all pulses was 20.25%. To address this, two independent assessors manually reviewed all of the MEP data to identify pulses where the automatic algorithm was ineffective. If the assessors concluded that the MEP algorithm had accurately detected the MEP onset as well as the positive and negative peaks of the MEP, then the amplitude and latency values calculated by the algorithm were retained. For the remaining trials, there were two possibilities:

1) The assessor was also unable to reliably identify the MEP characteristics. This could have been due to excessive muscle activity occurring before the TMS pulse, or significant artifacts throughout the EMG signal. In some cases, an MEP simply wasn't produced by the TMS pulse. In such cases, the pulse was discarded. Across all participants, an average of 6.93% of task-related pulses were discarded, with individual exclusion rates ranging from 0.0% to 16.25%. For rest pulses, the average exclusion rate was higher, at 14.66%, ranging from 0.0% to 30.00% across participants. When considering individual task conditions separately, the mean percentage of discarded pulses was 2.06%.
2) The accessor was able to visually identify the MEP onset and the positive and negative peaks, and manually correct the MEP latency and amplitude calculations. While the assessors followed the same general criteria as the algorithm, such as identifying the initial MEP deflection and the peak-to-peak values, they could make informed corrections in

cases where the algorithm misidentified these features due to signal noise, artifacts, or atypical MEP morphology. This approach enabled more accurate measurements in ambiguous or borderline cases. Final MEP latency and amplitude values were determined by averaging the results from both assessors.

Figure 3.5 illustrates an example MEP where the detection algorithm failed to correctly identify the MEP onset, but the assessors were able to manually correct the error.

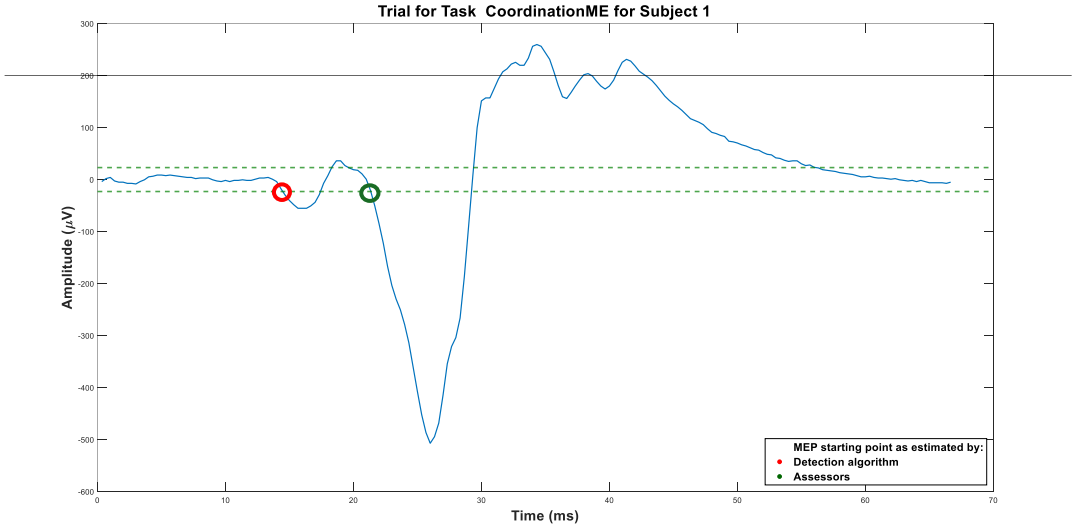

Figure 3. 5. An example of a valid MEP for Subject 1's Coordination$_{ME}$ task where the automatic detection algorithm was unable to accurately calculate the MEP amplitude and latency. In this case, the MEP onset was misidentified by the algorithm (red marker) due to a low signal-to-noise ratio or overlapping muscle activity masking the MEP response. Visual inspection by the assessors allowed the accurate selection of the MEP onset (the green marker) for this pulse (Image created by the author).

Standardization of MEP features

To account for inter-individual variability and allow for accurate comparison across conditions, the MEP latency values were normalized by dividing by the participant's height:

$$Standardized\ Latency = \frac{Latency\ (ms)}{\text{Height (cm)}}$$

The MEP amplitude values were standardized for each participant using the following equation:

$$Standardized\ Amplitude\ = \frac{MEPamplitude - MEPmin}{MEPmax - MEPmin}$$

where $MEPmin$ and $MEPmax$ represent the absolute minimum and maximum MEP amplitude values, respectively, in the dataset (across all five conditions) for that participant.

Rationale for standardization

Standardization was performed to account for individual differences in excitability and motor threshold variability, which can influence MEP characteristics. Rather than altering condition-related differences, this process ensured that inter-subject variability did not obscure meaningful effects. For MEP amplitudes, min-max scaling was applied separately for each participant, normalizing values to a 0–1 range across their entire dataset. This approach placed all participants' data on a common scale while preserving the relative distribution of values, ensuring that differences in individual scaling did not mask condition-related effects. For MEP latencies, normalization by height was used to account for differences in neural conduction time. This adjustment helped control for natural anatomical variability, allowing for a clearer comparison of latencies across conditions without introducing artificial distinctions.

Statistical analysis

To assess statistical differences among conditions, the Wilcoxon signed-rank test was applied due to the repeated measures design and non-normal distribution of the data. Effect sizes were calculated using Cohen's d to quantify the magnitude of the observed differences. Six pairwise

comparisons were performed: (1) $\text{Control}_{\text{ME}}$ vs. Rest, (2) $\text{Coordination}_{\text{ME}}$ vs. Rest, (3) $\text{Control}_{\text{MI}}$ vs. Rest, (4) $\text{Coordination}_{\text{MI}}$ vs. Rest, (5) $\text{Control}_{\text{MI}}$ vs. $\text{Coordination}_{\text{MI}}$, and (6) $\text{Control}_{\text{ME}}$ vs. $\text{Coordination}_{\text{ME}}$. Statistical significance, after Bonferroni correction, was considered for pairs with $p < 0.05$.

3.4.2 EEG data analysis

Classification problems

This study aimed to investigate whether EEG can be used to differentiate motor tasks targeting motor control versus motor coordination on a single-trial basis. Therefore, the main classification problems of interest were $\text{Control}_{\text{MI}}$ vs. $\text{Coordination}_{\text{MI}}$ and $\text{Control}_{\text{ME}}$ vs. $\text{Coordination}_{\text{ME}}$.

In addition, classification of each MI and ME task versus rest was also performed. It is well established that EEG can be used to distinguish MI and ME tasks from rest, so these classification problems were used to validate the implementation of the classification pipelines used, and to confirm that that the MI and ME tasks produced neural activation patterns that could be detected via EEG.

For the feature extraction and classification stages of the pipeline, different approaches were explored to try to maximize classification accuracy for the problems of interest. The effects of these factors on the classification accuracy of the different classification problems were investigated by statistical analysis.

Pre-processing

Pre-processing was performed using the EEGLAB toolbox in MATLAB and included re-referencing the data to the average of all EEG channels, downsampling from 500 Hz to 250 Hz,

and applying a 60 Hz notch filter to remove power line noise. Event markers were sent at the onset of the 4-second period during which participants performed the MI and ME task or remained at rest. These markers were used to extract task-relevant epochs for each trial. Specifically, a 4-second window was segmented for each trial, resulting in 60 epochs per condition (one per trial), each with dimensions of 1000 samples × 64 channels. These preprocessed epochs were used for further analysis.

Feature extraction

After extracting task-relevant epochs, features were computed for each epoch to capture relevant neural activity patterns. Given the complexity of brain signals during motor tasks, we investigated multiple types of features to identify those most effective for distinguishing between conditions. Different feature sets were explored to ensure robustness and to evaluate how various signal characteristics contributed to classification performance. When calculating the different types of features, in addition to considering the set of all 64 EEG channels collected (64_{ch}), we also considered a reduced set of 22 channels (22_{ch}) from key brain regions associated with motor tasks, specifically:

- Prefrontal cortex (Right: Fp2, F4, F8, AF4; Left: Fp1, F3, F7, AF3)
- Premotor cortex (Right: FC3, FC5, FC1, Left: FC4, FC6, FC2)
- Motor cortex (Right: C3, CP3, C1, CP1, Left: C4, CP4, C2, CP2)

Furthermore, to isolate specific neural oscillations associated with motor tasks and enhance the discriminative power of the features, we filtered the signal from each electrode into different frequency bands. The filtering was performed using a bandpass filter designed with the $extractBand$ function, which applies a zero-phase, FIR filter to preserve the temporal

characteristics of the signal. The filter order was set to 100, and the frequency band was defined by a minimum ($bandMin$) and maximum ($bandMax$) frequency, ensuring the filtered signal only included the desired frequency range. For each of the different sets of channels (64_{ch} and 22_{ch}), we considered two different sets of frequency bands:

- Five standard bands (5_{fb}): Delta (1–4 *Hz*), Theta (4–8 *Hz*), Alpha (8–13 *Hz*), Beta (13–30 *Hz*), and Gamma (30–80 *Hz*)
- Nine uniform bands (9_{fb}): Obtained by dividing the 4–40 *Hz* range into nine non-overlapping 4 *Hz* intervals: 4-8 *Hz*, 8-12 *Hz*, …, 36-40 *Hz*.

All features described in the following sections were calculated separately for all combinations of channel set (64_{ch} and 22_{ch}) and frequency band set (5_{fb} and 9_{fb}), for a total of four different combinations. All features were calculated for each extracted epoch.

FBCSP: The CSP algorithm is a widely utilized method for feature extraction in MI classification tasks [140]. Originally designed to discriminate between two classes of EEG data by maximizing variance for one class (e.g., $Control_{MI}$) while minimizing it for the other (e.g., Rest), CSP has demonstrated high efficacy in binary classification scenarios [141]. This helps to enhance the signal components that distinguish between the two classes while reducing noise and irrelevant signals.

In the FBCSP method, the CSP algorithm is applied separately to EEG signals that have been filtered into multiple frequency bands. This approach is advantageous because different frequency bands may capture distinct physiological processes that are relevant to the task at hand, improving the ability to discriminate between different conditions [112]. As mentioned above, the EEG data

from all 64 channels, as well as a subset of 22 channels, were first divided into five and nine frequency bands.

By using the FBCSP approach, the method capitalizes on the distinct characteristics of different frequency bands, allowing for a more comprehensive analysis of the EEG signals. This enhances the discriminative power of the features and potentially improves classification performance. Each frequency band contributes a unique set of features that can improve the ability to distinguish between task-related signals and resting states.

For each combination of channel set (64_{ch} or 22_{ch}) and frequency band set (5_{fb} or 9_{fb}), the CSP algorithm was applied to the signals from each frequency band. Specifically, 10 CSP spatial filters were used per frequency band —5 pairs of filters for the 5_{fb} case and 9 pairs for the 9_{fb} case—each maximizing the spatial variance between the two classes. For each of these spatial filters, the corresponding feature value was obtained by calculating the log-variance of the spatially filtered signals. This resulted in a total of 90 features for the 9_{fb} case and 50 features for the 5_{fb} case. With a total of 60 trials per class, this resulted in FBCSP feature matrices of dimension 120 by 50 (for 5_{fb}) and 120 by 90 (for 9_{fb}) for each binary classification problem explored. These values were then used as features for classification.

Functional connectivity measures (Correlation, Coherence, PLV)

To assess the potential of functional connectivity measures in enhancing classification accuracy, three different functional connectivity features (correlation, coherence, and PLV) were extracted. These measures were computed using MATLAB functions.

- **Correlation** between pairs of signals was computed using the $corr$ function in MATLAB, which calculates the Pearson correlation coefficient between signals from different channels.
- **Coherence** was measured using the $mscohere$ function to estimate the magnitude-squared coherence, which quantifies the degree of linear correlation between two signals in the frequency domain.
- **PLV** was computed to evaluate phase synchronization between pairs of channels. The phase of each channel's signal was extracted using the $Hilbert\ transform$. The PLV was then calculated as the mean of the complex exponential of the phase difference between the two signals.

Both amplitude-based relationships (correlation and coherence) and phase-based relationships (PLV) between signals from different electrodes or brain regions were considered. However, the features for each metric (correlation, coherence, and PLV) were treated separately for classification, not combined in the same feature set.

For each frequency band (i.e., within each set of channels), the functional connectivity metrics were calculated between channels within each trial. For the 64_{ch} set, this resulted in a 64x64 matrix per frequency band, with an upper triangular matrix of 2016 unique values representing the interdependencies between channels. The 2016 values for each frequency band were then concatenated into a 60 x 10080 feature matrix for the 5_{fb} case (i.e., 2016 features x 5 bands = 10080) and 60 x 18144 feature matrix for the 9_{fb} case (i.e., 2016 features x 9 bands = 18144), for each condition. For the 22_{ch} set, this resulted in a 22x22 matrix per frequency band, with an upper triangular matrix of 231 unique values representing the interdependencies between channels. The

231 values for each frequency band were then concatenated into a 60 x 1155 feature matrix for the 5_{fb} case (i.e., 231 features x 5 bands = 1155) and 60 x 2079 feature matrix for the 9_{fb} case (i.e., 231 features x 9 bands = 2079), for each condition.

We also attempted to calculate the mean functional connectivity within each ROI and use those values as features. For each trial, this method generated six values, corresponding to the three regions in both the right and left hemispheres, representing the average connectivity within the defined ROIs. These averaged values were intended to capture the interdependencies within the regions and were used as features for classification. This resulted in a 60 x 30 feature matrix for the 5_{fb} case (i.e., 60 trials x 6 ROIs x 5 bands) and a 60 x 54 feature matrix for the 9_{fb} case (i.e., 60 trials x 6 ROIs x 9 bands). However, the performance did not meet expectations, so these results were excluded from the final analysis.

Feature selection

For all of the feature pools considered (CSP, correlation, coherence, and PLV, for each combination of channel set and frequency band set), the mRMR method was used to select the most informative features. Feature subsets with dimensionalities of 10, 20, 30, 40 were considered, along with all available features for the particular scenario (i.e., 50 for the 5_{fb} cases and 90 for the 9_{fb} cases), enabling a comparison of classifier performance with different numbers of features.

Classification

For all scenarios (i.e., all combinations of channel sets, frequency band sets, feature types, and feature set sizes), three classifiers were employed: LDA, Support Vector Machine (SVM), and Decision Tree. The LDA classifier was selected for its simplicity and efficiency in distinguishing between motor tasks. The SVM classifier, with a radial basis function (RBF) kernel, was used to

capture potential nonlinear relationships within the data. The hyperparameters of the SVM were optimized through grid search within each training fold. Additionally, the Decision Tree classifier was employed to further assess the performance of the extracted features, with tree depth and splitting criteria fine-tuned through cross-validation to prevent overfitting. The classification was done in MATLAB using the $fitcdiscr$, $fitcsvm$, and $fitctree$ functions for LDA, SVM, and Decision Tree classifiers, respectively. Classifier performance was estimated using 5-fold cross-validation, implemented using *cvpartition* in MATLAB. For each fold, feature extraction (for FBCSP features only), feature selection, and classifier training were performed exclusively on the training data. This approach prevented data leakage and ensured unbiased performance evaluation. The process was repeated over 15 independent runs, and the resulting classification accuracies were averaged to minimize the impact of random variations and improve the reliability of the results [142]. This multi-classifier approach aimed to provide a more comprehensive evaluation of the extracted feature set, offering potential insights into the discriminative power of FBCSP and functional connectivity features across different classification methods.

Summary of investigated scenarios

A total of 240 classification scenarios were explored, considering various parameter combinations:

- **Feature types:** FBCSP, correlation, coherence, and PLV
- **Frequency band sets:** 5_{fb} and 9_{fb}
- **Channel sets:** 64_{ch} set and 22_{ch} set
- **Feature set sizes:** selected feature sets of 10, 20, 30, 40, and all features
- **Classifiers:** LDA, SVM, and Decision Tree

Each classification scenario was implemented using a 5-fold cross-validation approach, ensuring reliable performance evaluation. The complete analysis pipeline, including preprocessing, feature extraction, selection, and classification, is illustrated in Figure 3.6.

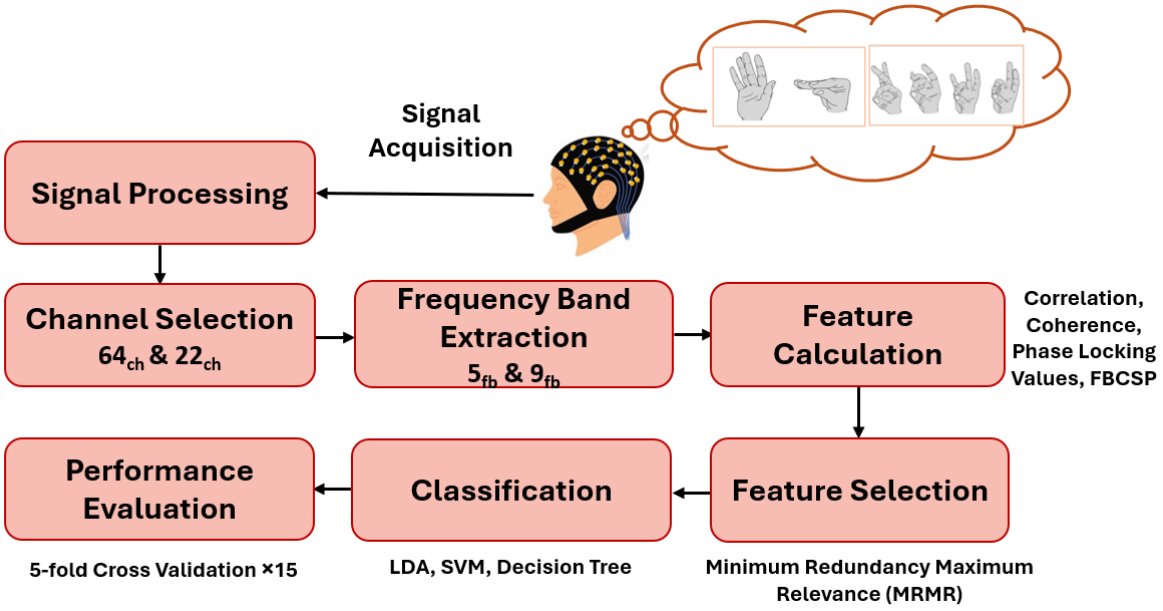

Figure 3. 6. EEG Workflow: Signal acquisition, processing, feature extraction, and classification to identify neural patterns (Image created by the author).

3.5 Statistical analysis

To determine the effects of the different classification approaches investigated on the ability to distinguish the control and coordination tasks, we used the Friedman test, a non-parametric alternative to repeated-measures ANOVA. This test was used to determine the effect of i) feature type, ii) frequency band set, iii) channel set, iv) feature set size, and v) classifier on overall accuracy across the two classification problems of interest (i.e, $Control_{ME}$ vs. $Coordination_{ME}$ and $Control_{MI}$ vs $Coordination_{MI}$). For each factor, the different levels of that factor were compared based on the average accuracy across all scenarios (i.e., all combinations of the other factors, and

both classification problems) for each of the 21 participants. If the Friedman test revealed a significant effect for a given factor, Dunn-Sidak post-hoc tests were conducted to determine specific pairwise differences between levels of that factor. Based on the results of these analyses, a "best" overall classification pipelines were selected and the classification results for this pipeline were further analyzed.

Classification accuracies for 1) $Control_{ME}$ vs. $Coordination_{ME}$, and 2) $Control_{MI}$ vs $Coordination_{MI}$ for the "best" overall classification pipeline were determined. To determine if these accuracies were significantly different from chance, the classification process was repeated after first randomizing the class labels, creating a distribution representing the ''chance" level classification accuracy. For each of the two classification problems, Wilcoxon signed-rank tests were performed to compare the "real" to the "random" accuracies. A Wilcoxon signed-rank test was also used to compare the accuracy for $Control_{MI}$ vs. $Coordination_{MI}$ with that for $Control_{ME}$ vs. $Coordination_{ME}$.

The same analysis was performed for the four "Motor Task vs. Rest" classification problems (i.e, $Control_{ME}$ vs. Rest, $Coordination_{ME}$ vs. Rest, $Control_{MI}$ vs. Rest, and $Coordination_{MI}$ vs. Rest). That is, Friedman tests (with post-hoc pairwise Dunn-Sidak tests) were used to determine the effect of i) channel set, ii) frequency band set, iii) feature type, iv) feature set size, and v) classifier on overall accuracy across the four classification problems. For each factor, the different levels of that factor were compared based on the average accuracy across all scenarios (i.e., all combinations of the other factors, and the four Motor Task vs. Rest classification problems) for each of the 21 participants. Based on the results of these analyses, a "best" overall classification pipeline was selected for the Motor Task vs. Rest classification problems. These results were compared to results obtained using random labels, and Wilcoxon signed-rank tests were used to compare the

"real" to the "random" accuracies. Wilcoxon signed-rank tests were also used to perform pairwise comparisons of the four Motor Task vs. Rest accuracies. Statistical significance, after Bonferroni correction, was considered for pairs with $p < 0.05$.

Chapter 4 Results

4.1 TMS/EMG results: MEP amplitude and latency analysis

MEPs were analyzed to assess corticospinal excitability and conduction time across five conditions: $Control_{MI}$, $Coordination_{MI}$, $Control_{ME}$, $Coordination_{ME}$, and Rest. The primary outcome measures were MEP amplitude and latency, standardized across all participants. Boxplots in Figures 4.1 and 4.2 illustrate the distribution of MEP amplitudes (raw values) and latencies (standardized values), respectively, across the five conditions. The boxes represent the interquartile range (IQR), while the horizontal lines indicate the medians, and the whiskers extend to the maximum and minimum datapoints. For both amplitude and latency, pairwise comparisons between conditions were conducted using the Wilcoxon signed-rank test, suitable for non-parametric repeated-measures data. There were eight comparisons of interest: each of the four task conditions with rest (4), MI with ME within each targeted motor function (2), and control with coordination within imagery and execution (2). Bonferroni correction was applied to control for multiple comparisons ($\alpha = 0.05$); significant pairwise differences are annotated accordingly in the plots. In addition to p-values, Rank-biserial correlation coefficients (*rb*) were calculated to quantify the magnitude of observed effects. This non-parametric effect size measure complements the Wilcoxon signed-rank tests by indicating the strength of the differences between condition pairs. Figure 4.3 and Table 4.1 provide an alternate representation, showing the overall mean differences in MEP amplitude (in μV) and latency (in *ms*) for each task condition compared to rest.

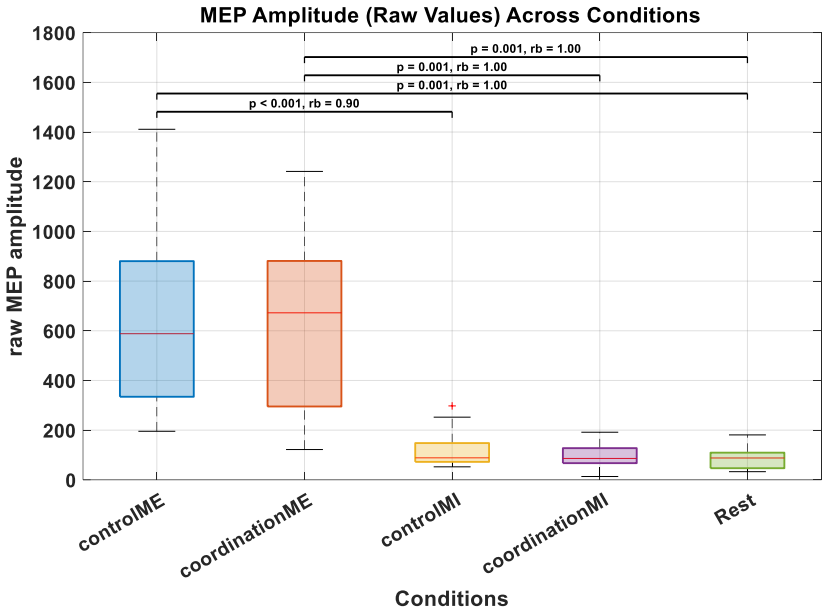

Figure 4. 1. Raw MEP amplitudes across all subjects for each condition. Boxplots show the distribution after outlier removal using the IQR method. Significant differences between specific condition pairs (Bonferroni-adjusted $\alpha = 0.05$) are annotated. P-values are based on Wilcoxon signed-rank tests with Bonferroni correction. Rank-biserial correlation values (*rb*) are reported as a non-parametric effect size measure.

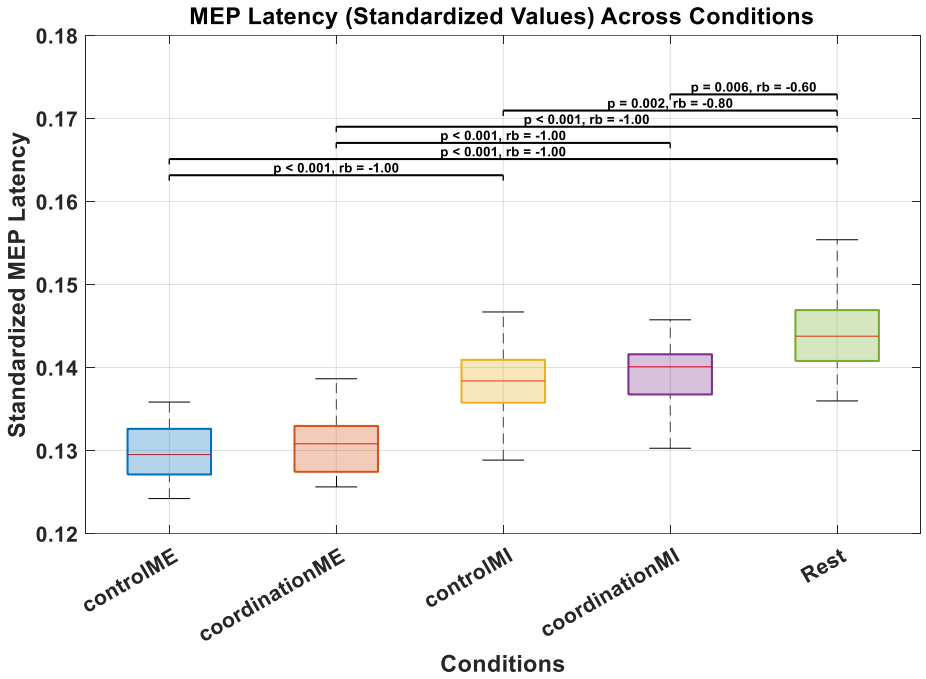

Figure 4. 2. Standardized MEP latencies across all subjects for each condition. Boxplots show the distribution after outlier removal using the IQR method. Significant differences between specific condition pairs (Bonferroni-adjusted $\alpha = 0.05$) are annotated. P-values are based on Wilcoxon signed-rank tests with Bonferroni correction. Rank-biserial correlation values (*rb*) are reported as a non-parametric effect size measure.

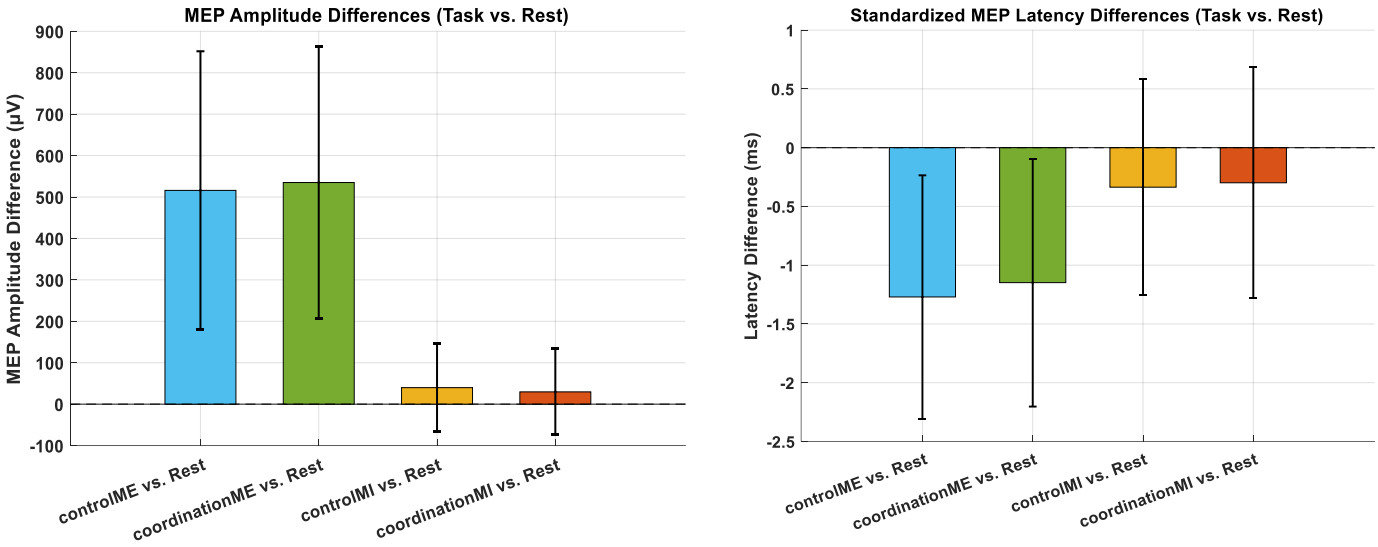

a) **b)**

Figure 4. 3. Mean differences in MEP amplitude (raw values) and latency (standardized values) for each task condition compared to rest. a) Positive values indicate greater MEP amplitude during the task condition. b) Negative values indicate longer latency during the task condition relative to rest. Error bars represent standard deviation across subjects.

Table 4. 1. MEP Amplitude and Standardized MEP Latency Differences (Task - Rest)

Task Condition	**MEP Amplitude Difference (*μV*)**	**Standardized MEP Latency Difference (*ms*)**
$Control_{ME}$ vs. Rest	515.96 ± 335.83	-1.27 ± 1.03
$Coordination_{ME}$ vs. Rest	534.97 ± 327.33	-1.14 ± 1.05
$Control_{MI}$ vs. Rest	39.90 ± 106.01	-0.33 ± 0.91
$Coordination_{MI}$ vs. Rest	29.66 ± 104.02	-0.29 ± 0.98

4.2 EEG analysis results:

4.2.1 Classification parameter effects – identifying "best" pipelines

Figures 4.4.a and 4.4.b summarize the classification performance across 21 participants for both the Control vs. Coordination (left side of the figure) and the Motor Task vs. Rest (right side of the figure) classification problems. It shows the distribution of the overall average classification accuracies achieved for the different a) channel sets, b) frequency bands, c) feature types, d) number of selected features, and e) classifiers across all classification scenarios explored for each problem. Statistically significant differences identified using post-hoc Dunn-Sidak tests are indicated on the plots, along with the corresponding *p*-values.

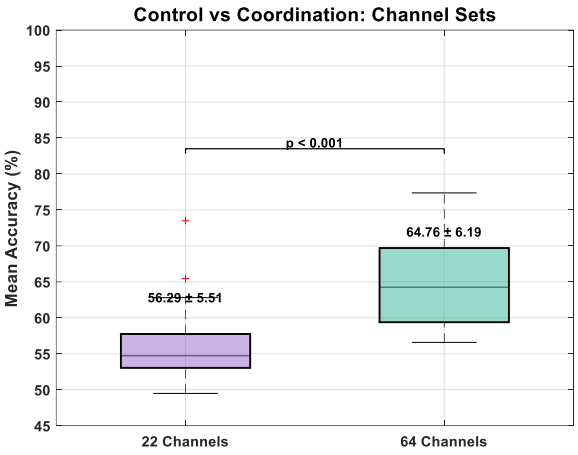

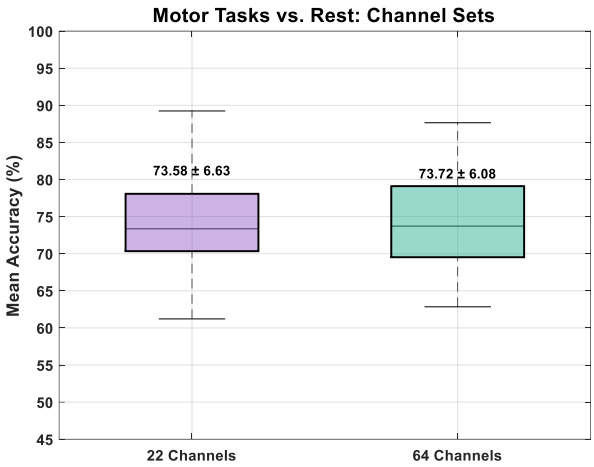

i)

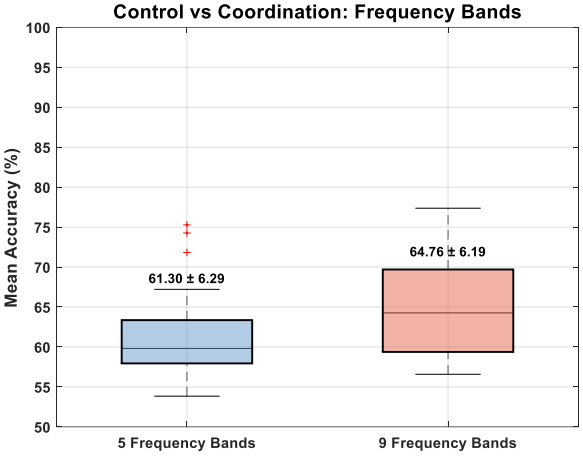

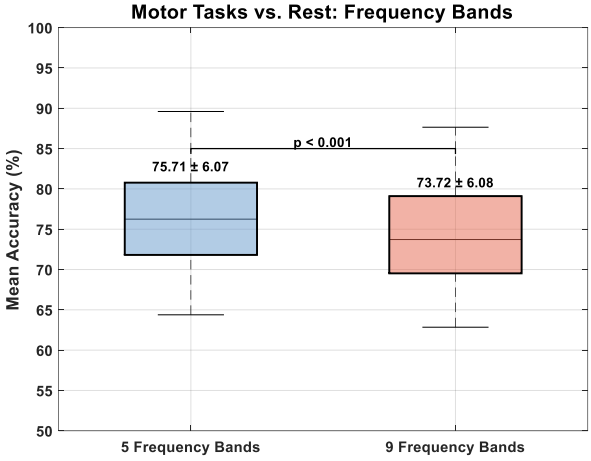

ii)

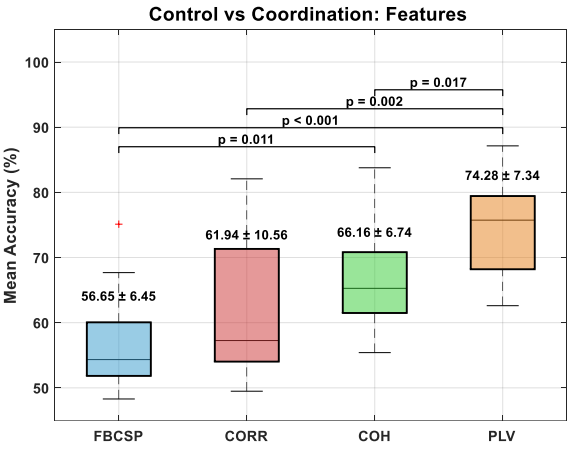

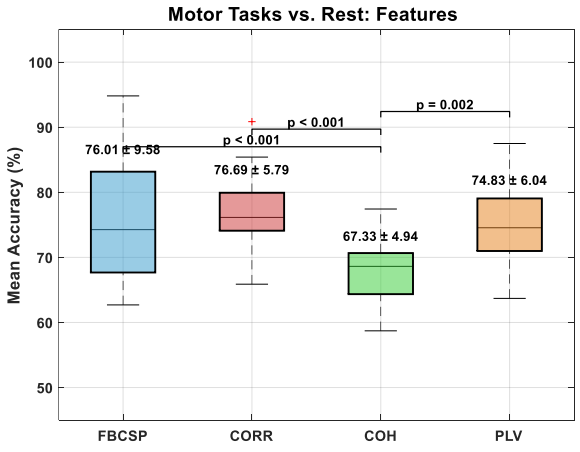

iii)

Figure 4. 4.a. Boxplots showing the distribution of classification accuracies for the Control vs. Coordination (left) and Motor Tasks vs. Rest (right) classification problems, for the different (i) channel configurations, (ii) number of frequency bands, and (iii) feature types explored. Significant differences ($p < 0.05$) are indicated on the figures; p-values were computed using the post-hoc Dunn-Sidak tests.

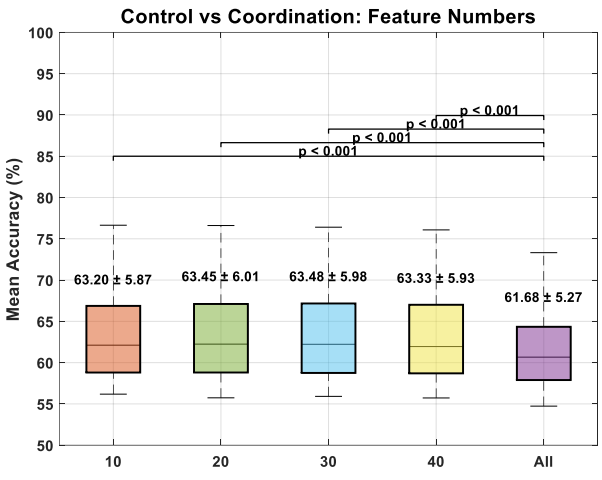

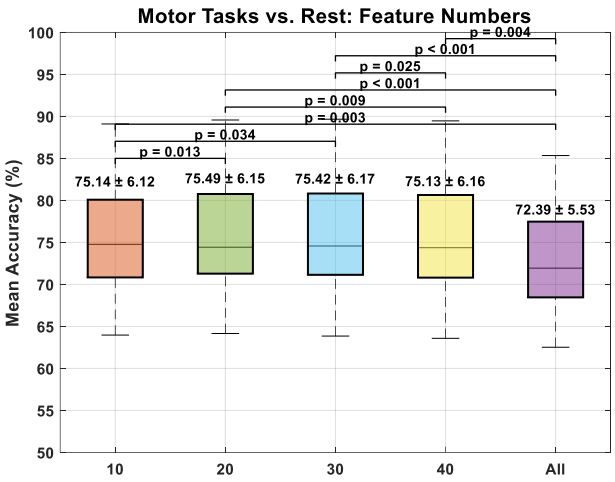

i)

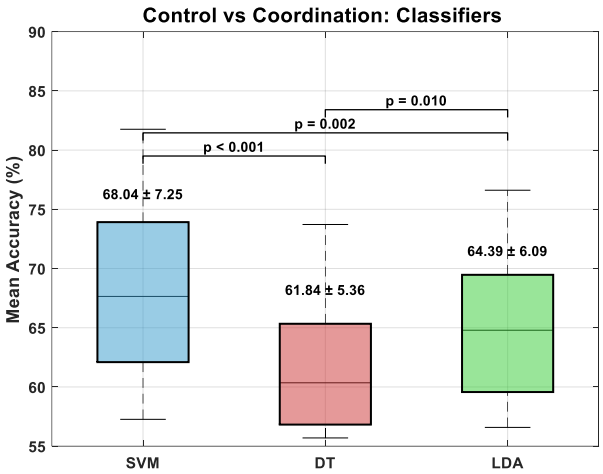

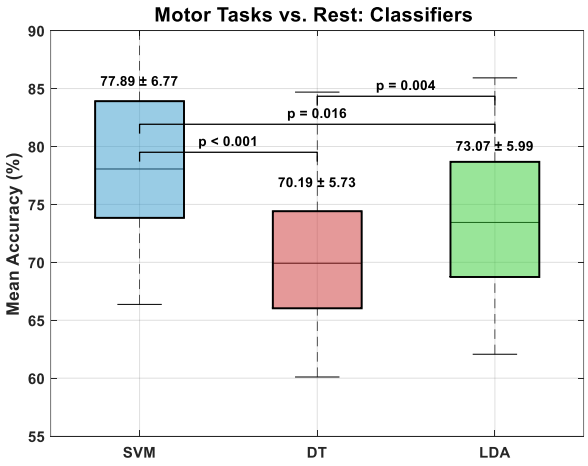

ii)

Figure 4.4.b. Boxplots showing the distribution of classification accuracies for the Control vs. Coordination (left) and Motor Tasks vs. Rest (right) classification problems, for the different (i) feature set sizes and (ii) classifiers explored. Significant differences ($p < 0.05$) are indicated on the figures; p-values were computed using the post-hoc Dunn-Sidak tests.

Based on these results, the "best" pipeline was determined for the two Coordination vs. Control classification problems, and for the four Motor Task vs. Rest classification problems, as follows:

- **Control vs. Coordination:** The best performance was achieved using 64 channels (64_{ch}), with PLV features calculated over the nine frequency bands (9_{fb}), and with an SVM classifier based on 30 selected features.
- **Motor tasks vs. Rest:** The best performance was achieved using 22 channels (22_{ch}), with FBCSP features calculated over the five frequency bands (5_{fb}), and with an SVM classifier based on 20 selected features.

In cases where there was no statistically significant difference in accuracy amongst different levels of a factor, the one with the highest average accuracy value was selected.

4.2.2 Classification accuracies for the Control vs. Coordination classification problems

Figure 4.5 presents the distribution of classification accuracies across the 21 participants for the two binary Control vs Coordination classification problems (i.e., $Control_{ME}$ vs. $Coordination_{ME}$ and $Control_{MI}$ vs. $Coordination_{MI}$) using the "best" pipeline identified in section 4.2.1. Accuracies obtained for all four classification problems were significantly different from chance, based on the comparison to the distribution obtained using random labels ($p<0.001$). Significant differences between classification problems, as assessed using Wilcoxon signed-rank tests, are indicated on the plot.

Table 4.2 shows the mean accuracies for the classification analysis performed with true and randomized labels for each Control vs Coordination classification problem, along with the *p*-value from the comparison.

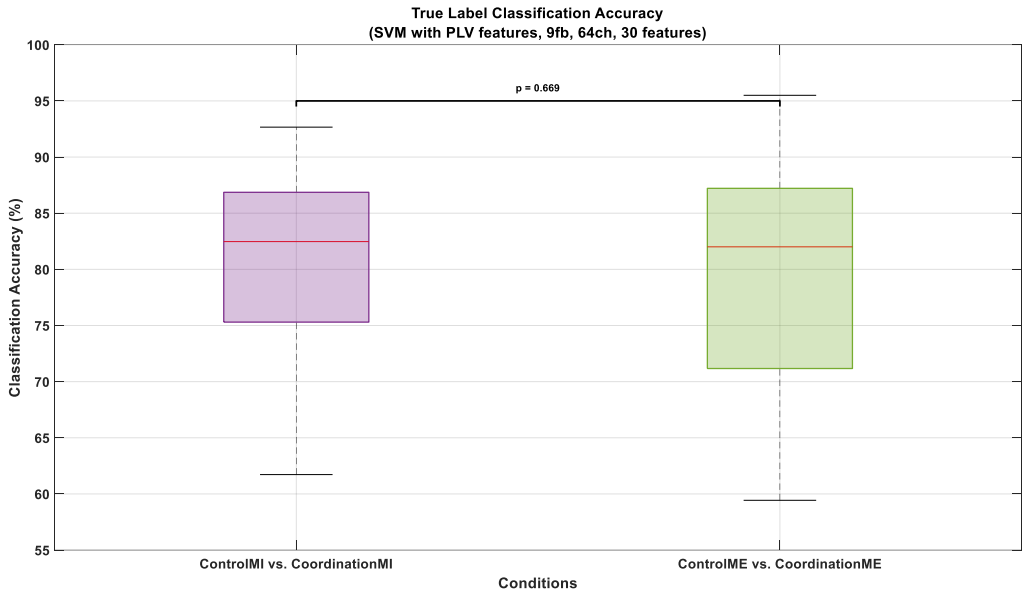

Figure 4. 5. Accuracies for the Control vs. Coordination classification problems, using the "best" pipeline identified in section 4.2.1 (SVM classifier with PLV features, 9_{fb}, 64_{ch}, 30 features). Accuracies obtained for the ME and MI scenarios were not significantly different based on the Wilcoxon signed-rank test.

Table 4. 2. Classification Accuracies for the two Control vs Coordination classification problems, with true and randomized labels.

Condition	True Labels (mean ± std)	Random Labels (mean ± std)	p-value
$Control_{ME}$ vs. $Coordination_{ME}$	82.7 ± 8.7	48.8 ± 4.3	<0.001
$Control_{MI}$ vs. $Coordination_{MI}$	80.5 ± 9.6	51.0 ± 3.1	<0.001

Figure 4.6 shows the classification accuracies for each participant in the two Control vs Coordination classification problems using the "best" pipeline determined in section 4.2.1. A threshold of 58.3%, determined via the binomial test based on 60 samples per class, was used to determine whether individual classification accuracies significantly exceeded chance.

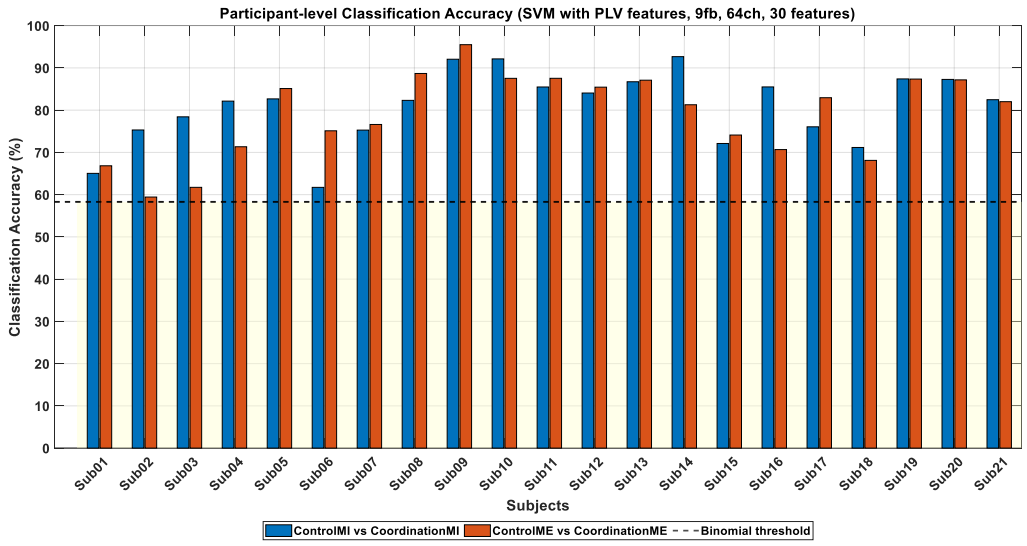

Figure 4. 6. Participant-level classification accuracies for $Control_{ME}$ vs. $Coordination_{ME}$ and $Control_{MI}$ vs. $Coordination_{MI}$ across 21 subjects using the "best" pipeline identified in section 4.2.1 (SVM classifier with PLV features, 9_{fb}, 64_{ch}, 30 features). The dashed horizontal line at 58.3% denotes the binomial test threshold for statistical significance, calculated based on 60 samples per class. Classification accuracies above this threshold are considered significantly greater than chance.

4.2.3 Classification accuracies for the Motor Task vs. Rest classification problems

Figure 4.7 presents the distribution of classification accuracies for each of the four binary Motor Task vs. Rest classification problems (i.e., $Control_{ME}$, $Coordination_{ME}$, $Control_{MI}$, and $Coordination_{MI}$ vs. Rest) using the "best" pipeline identified in section 4.2.1. Accuracies obtained for all four classification problems were significantly different from chance, based on the comparison to the distribution obtained using random labels ($p<0.001$). Significant differences between classification problems, as assessed using Wilcoxon signed-rank tests with Bonferroni correction, are indicated on the plot.

Table 4.3 shows the mean accuracies for the classification analysis performed with true and randomized labels for each Motor Task vs. Rest classification problem, along with the p-value from the comparison with the true accuracies.

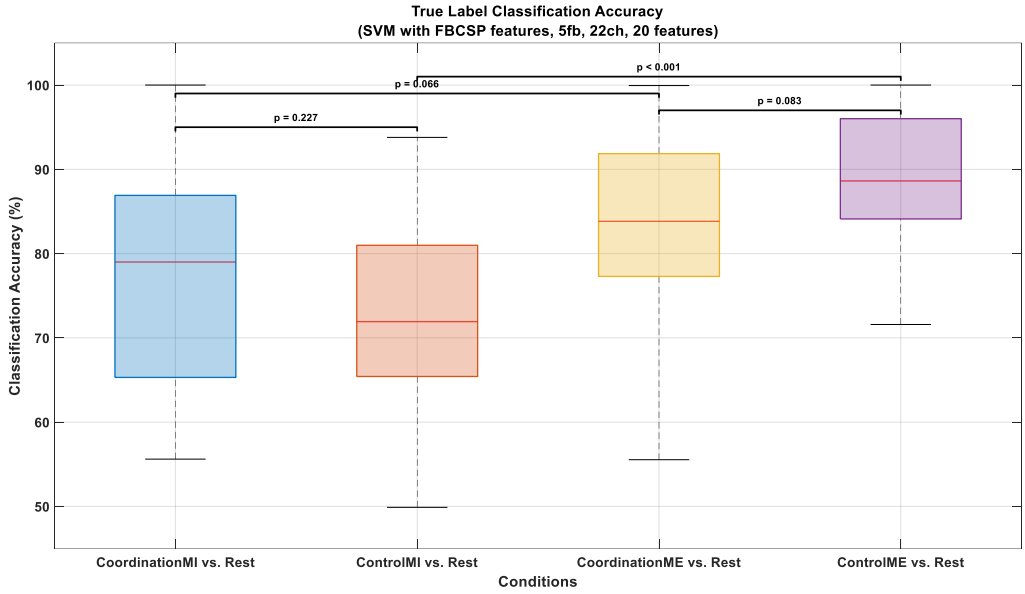

Figure 4. 7. Accuracies for the Motor Task vs. Rest classification problems, using the "best" pipeline identified in section 4.2.1 (SVM classifier with FBCSP features, 5_{fb}, 22_{ch}, 20 features). P-values are based on the Wilcoxon signed-rank test with Bonferroni correction for pairwise comparisons.

Table 4. 3. Classification Accuracies for the four Motor Task vs. Rest classification problems, with true and randomized labels.

Condition	True Labels (mean ± std)	Random Labels (mean ± std)	p-value
$Control_{ME}$ vs. Rest	88.7 ± 7.4	50.7 ± 4.4	<0.001
$Coordination_{ME}$ vs. Rest	83.4 ± 10.4	49.8 ± 5.1	<0.001
$Control_{MI}$ vs. Rest	72.0 ± 11.0	50.2 ± 5.1	<0.001
$Coordination_{MI}$ vs. Rest	76.6 ± 12.2	49.4 ± 6.3	<0.001

Figure 4.8 shows the classification accuracies for each participant in the four Motor Task vs. Rest classification problems using the "best" pipeline determined in section 4.2.1. A threshold of 58.3%,

determined via the binomial test based on 60 samples per class, was used to determine whether individual classification accuracies significantly exceeded chance.

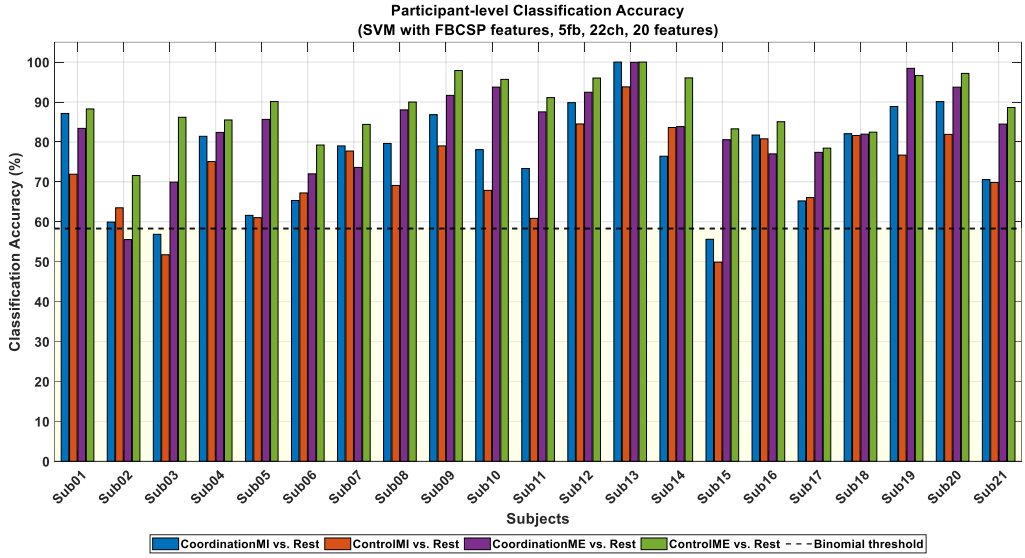

Figure 4. 8. Participant-level classification accuracies for $Control_{ME}$, $Coordination_{ME}$, $Control_{MI}$, $Coordination_{MI}$ vs. Rest across 21 subjects using the" best" pipeline identified in section 4.2.1 (SVM with FBCSP features, 5_{fb}, 22_{ch}, 20 features). The dashed horizontal line at 58.3% denotes the binomial test threshold for statistical significance, calculated based on 60 samples per class. Classification accuracies above this threshold are considered significantly better than chance.

Chapter 5 Discussion

5.1 Assessing CSE via MEPs during MI and ME

One of the primary objectives of this preliminary study was to evaluate whether MI tasks, specifically those designed to target motor coordination and motor control, can enhance CSE, as measured by TMS-evoked MEPs. This was investigated using TMS-EMG recordings in healthy participants during both MI and ME tasks. To address this goal, we designed and implemented two MI tasks ($Control_{MI}$ and $Coordination_{MI}$) and two ME tasks ($Control_{ME}$ and $Coordination_{ME}$), each reflecting distinct motor demands. MEP amplitude and latency served as neurophysiological markers of excitability and conduction efficiency, respectively. MEP amplitude was analyzed using raw values to directly capture changes in CSE. In contrast, latency values were standardized to account for individual differences in baseline conduction speed, ensuring comparability across participants. The MEP amplitude and latency results revealed distinct neuromodulatory patterns associated with targeted motor function (coordination vs. control) and with task type (MI vs. ME). Figures 4.1 and 4.2 show that the Rest condition exhibited the lowest MEP amplitude (106.84 ± 69.20 μV) and longest latency (0.14 ± 0.009) on average, reflecting lower excitability and slower conduction during this passive state.

For ME tasks, both conditions demonstrated significantly higher MEP amplitudes compared to Rest ($Control_{ME}$: 622.80 ± 340.10 μV, $p < .001$; $Coordination_{ME}$: 641.81 ± 346.99 μV, $p < .001$), indicating an increase in excitability during active movement. Similarly, both ME conditions demonstrated significantly reduced latencies relative to Rest ($Control_{ME}$: 0.12 ± 0.003, $p < .001$; $Coordination_{ME}$: 0.13 ± 0.003, $p < .001$), indicating decreased conduction time during active movement.

For MI tasks, neither of the conditions exhibited a statistically significant increase in MEP amplitude relative to Rest ($Control_{MI}$: 146.74 ± 144.30, $p = 0.35$; $Coordination_{MI}$: 136.50 ± 138.48,

p =0.24). However, both MI conditions demonstrated statistically significant reductions in standardized latency relative to Rest ($Control_{MI}$: 0.13 ± 0.005, *p = 0.002*; $Coordination_{MI:}$ 0.13 ± 0.003, *p = 0.006*), suggesting that MI facilitated faster signal transmission in both tasks. No statistically significant differences were found between $Control_{MI}$ and $Coordination_{MI}$ for either MEP amplitude (*p = 0.93*) or latency (*p = 1.00*). Likewise, $Control_{ME}$ and $Coordination_{ME}$ did not differ significantly in MEP amplitude (*p = 1.00*) or latency (*p = 0.23*). Figure 4.3 and Table 4.1 further illustrate the average differences in MEP amplitude and standardized latency between each task condition and rest.

These results demonstrated neuromodulatory differences between task types and conditions. The Rest condition consistently showed the lowest MEP amplitude and longest latency, reflecting reduced excitability and slower corticospinal conduction during the passive state. Both ME tasks significantly increased MEP amplitude and decreased latency relative to Rest, confirming that actual movement robustly enhances motor CSE and signal conduction speed. This aligns with well-established findings in the literature demonstrating that voluntary movement potentiates corticospinal output [143].

While both MI conditions produced significant latency reductions relative to Rest, no differences in amplitude or latency were observed between the control and coordination variants within either MI or ME tasks. The absence of amplitude differences between $Control_{MI}$ and $Coordination_{MI}$ suggests that imagining control versus coordination motor sequences may not differentially modulate CSE, at least as measured by MEP amplitude in this cohort. Similarly, the comparable excitability between $Control_{ME}$ and $Coordination_{ME}$ may reflect that both executed tasks, despite differences in motor demands, recruited overlapping motor networks sufficiently to elicit similar corticospinal responses.

Several factors may explain these findings. First, the lack of significant amplitude modulation during MI may be attributed to variability in imagery ability and task engagement across participants. Previous studies have reported mixed results regarding MI-induced MEP amplitude changes; some found increases, whereas others reported minimal or inconsistent modulation, often linked to individual differences in imagery vividness and attentional focus [144]. The relatively simple nature of the imagined tasks may not have imposed sufficient cognitive or motor demands to evoke amplitude changes. Conversely, the significant latency reductions during MI suggest that imagery facilitates faster neural conduction, possibly by priming motor circuits and enhancing signal transmission efficiency even without overt muscle activation. This aligns with studies demonstrating that MI engages motor-related cortical and subcortical regions, modulating corticospinal pathways and influencing conduction time [63], [64], [54], [145].

The lack of significant differences between the $Control_{MI}$ and $Coordination_{MI}$ conditions may also reflect shared neural mechanisms underlying both tasks. Neuroimaging evidence shows overlapping activation of motor areas during MI of both simple and complex movements [146]. While coordination may engage additional higher-order areas, this may dilute corticospinal facilitation detectable via MEP amplitude, as these ancillary networks may not directly modulate corticospinal output.

5.2 EEG-based differentiation of MI tasks

The second major goal of this study was to investigate whether EEG signals can be used to distinguish between MI tasks targeting motor control and coordination on a single-trial basis. To address this, we designed a classification pipeline, investigating multiple channel sets, frequency bands, feature types, number of selected features, and classifiers. This multifactorial design

allowed us to systematically evaluate which processing parameters most effectively differentiate these MI conditions in healthy participants.

To achieve this goal, EEG data were processed using two electrode configurations (64_{ch} and 22_{ch} sets), and two different sets of frequency bands (5_{fb} and 9_{fb} sets). Features were extracted using both conventional spatial filtering techniques (e.g., FBCSP) and functional connectivity measures (e.g., correlation, coherence, and PLV). Additionally, we evaluated the effects of selecting different feature set sizes using the automatic feature selection algorithm mRMR, and of using three different classical machine learning models: LDA, SVM, and Decision Trees. These analyses were intended not only to maximize classification accuracy but also to identify scalable and interpretable strategies suitable for future BCI development. Figure 4.4.a and 4.4.b present boxplots showing the distribution of classification accuracies for the Coordination vs. Control (left) and the Motor Task vs. Rest (right) classification problems across the different scenarios explored.

5.2.1 Classification accuracies for the Control vs. Coordination classification problems

For the more challenging classification of the Control vs. Coordination tasks, the 64_{ch} setup yielded significantly better performance than the 22_{ch} configuration ($64.76 \pm 6.19\%$ vs. $56.29 \pm 5.51\%$, $p < .001$). This highlights the value of full-head coverage in detecting more nuanced neural signatures associated with complex motor intentions. While the 9_{fb} configuration offered higher accuracy ($64.76 \pm 6.19\%$) than 5_{fb} ($61.30 \pm 6.29\%$), the difference was not statistically significant. In terms of features, PLV demonstrated the highest performance ($74.28 \pm 7.34\%$), significantly outperforming CORR ($61.94 \pm 10.56\%$, $p = 0.002$), COH ($66.16 \pm 6.74\%$, $p = 0.017$), and FBCSP ($56.65 \pm 6.45\%$, $p < .001$). These findings emphasize the potential of phase-based connectivity features in capturing the timing relationships critical for differentiating coordinated from

controlled movement, supporting emerging literature on PLV's role in high-level motor representations [147]. The best accuracy was achieved using 30 features (63.48 ± 5.98%, $p < .001$), reinforcing the idea that a moderate number of well-chosen features is optimal. Among classifiers, SVM outperformed both LDA and Decision Tree (68.04 ± 7.25% vs. 64.39 ± 6.09%, $p = 0.002$ and 61.84 ± 5.36%, $p = 0.01$, respectively), further validating its suitability for EEG-based motor decoding across both task types [125], [126], [148].

Statistical comparisons using the Friedman test with Dunn-Sidak post hoc corrections were conducted to evaluate the effects of different factors—channel configurations, number of frequency bands, feature types, feature set sizes, and classifiers—on classification performance. We assessed the relative performance of each option within each factor across all scenarios. Based on these comparisons, the SVM classifier, PLV features, 9_{fb} setup, 64_{ch} configuration, and 30 selected features emerged as the most effective options overall for distinguishing between $Control_{ME}$ vs. $Coordination_{ME}$ and $Control_{MI}$ vs. $Coordination_{MI}$ tasks.

With this" best" pipeline, $Control_{ME}$ and $Coordination_{ME}$ were classified with a mean accuracy of 82.7 ± 8.7%, while $Control_{MI}$ and $Coordination_{MI}$ were classified with an accuracy of 80.5 ± 9.6%, see Figure 4.5 and Table 4.2. Both results significantly exceeded their respective chance-level baselines (~49–51%), which were determined through permutation testing with randomly shuffled labels. This demonstrates that coordination and control engage distinct, decodable neural processes, not only during movement execution but also during internally imagined movement.

Further analysis of individual classification accuracies, as shown in Figure 4.6, revealed that all participants exceeded the statistical threshold for chance performance (58.3%) in both ME and MI conditions. Accuracy ranged from 59.4% to 95.5% ($SD = 8.7\%$) in the ME condition and from 61.7% to 92.6% ($SD = 9.6\%$) in the MI condition. Notably, 19 out of 21 participants (90.5%)

achieved classification accuracies above 70% in the MI tasks, and 17 out of 21 participants (81.0%) exceeded this threshold in the ME tasks. This consistently high performance, along with the relatively low standard deviations, underscores the robustness of the neural distinctions between control and coordination and highlights their potential for generalization across individuals.

Overall, the Control vs. Coordination classification results serve two critical purposes: first, they demonstrate that each motor condition, executed or imagined, elicits distinct EEG patterns that are robustly and reliably separable; second, the lack of a significant difference in classification performance between ME and MI conditions ($p = 0.66$) suggests that the neural representations of control and coordination tasks are comparably encoded across both modes, meaning that the brain processes or represents these tasks in a similar way during both ME and MI. Importantly, the similarity in neural encoding may support the potential of MI as an effective substitute for ME in training or rehabilitation contexts, where physical movement may be limited.

5.2.2 Classification accuracies for the Motor Task vs. Rest classification problems

In the classification of Motor Tasks vs. Rest, the 64_{ch} EEG layout yielded a slightly higher accuracy ($73.72 \pm 6.08\%$) compared to the reduced 22_{ch} configuration ($73.58 \pm 6.63\%$); however, this difference was not statistically significant. This suggests that while dense spatial sampling may offer minor gains, even reduced channel sets can be adequate for this task. Regarding frequency bands, the 5_{fb} configuration significantly outperformed the 9_{fb} setup ($75.71 \pm 6.07\%$ vs. $73.72 \pm 6.08\%$, $p < .001$). The 5_{fb} set provided better generalization, likely due to reduced overfitting and improved simplicity, which aligns with findings from prior BCI research recommending fewer bands for efficient decoding [121]. Feature type comparison showed that CORR features provided the highest accuracy ($76.69 \pm 5.79\%$), slightly exceeding FBCSP

(76.01 ± 9.58%) and PLV (74.83 ± 6.04%), while COH lagged behind (67.33 ± 4.94%). Despite close values between CORR and FBCSP, statistical results and existing literature highlight FBCSP's widespread application and robustness in MI classification [121]. Feature set size analysis revealed that performance peaked when using 20 features (75.49 ± 6.15%, $p < .05$), after which no meaningful gain was observed. Lastly, SVM achieved the highest classification performance (77.89 ± 6.77%), significantly outperforming both LDA (73.07 ± 5.99%, $p = 0.01$) and Decision Tree (70.19 ± 5.73%, $p < .001$) [148], [126]. SVM's superior accuracy is likely due to its effectiveness in handling high-dimensional EEG data and its robustness with relatively small training sets [125].

Statistical comparisons using the Friedman test with Dunn-Sidak post hoc corrections were conducted to evaluate the effects of different factors on classification performance. We assessed the relative performance of each option within each factor across all scenarios. Based on these comparisons, the SVM classifier, FBCSP features, 5_{fb} setup, 22_{ch} configuration, and 20 selected features emerged as the most effective options overall for distinguishing between $Control_{ME}$, $Coordination_{ME}$, $Control_{MI}$, and $Coordination_{MI}$ vs. Rest.

With this" best" pipeline, $Control_{ME}$ vs. Rest (88.7 ± 7.4%) yielded a higher mean accuracy than $Coordination_{ME}$ vs. Rest (83.4 ± 10.4%), though the difference was not statistically significant ($p=0.083$), see Figure 4.7 and Table 4.3. This trend is consistent with expectations, as actual physical movement typically produces strong, well-defined EEG patterns distinguishable from rest. Conversely, in the MI conditions, the accuracy for $Control_{MI}$ vs. Rest (72.0 ± 11.0%) was lower than for $Coordination_{MI}$ vs. Rest (76.6 ± 12.2%), though again the difference was not statistically significant ($p=0.227$). When comparing imagery and execution within the same task type, $Control_{ME}$ was distinguishable from Rest with significantly higher accuracy than $Control_{MI}$

($p<0.001$). However, this was not the case for the coordination task ($p=0.066$), suggesting that $\text{Coordination}_{\text{MI}}$ may elicit neural patterns that are more similar in structure and strength to those generated during $\text{Coordination}_{\text{ME}}$. This could be due to the greater cognitive and sensorimotor demands involved in coordinating imagined actions [42].

Further analysis of individual classification accuracies, as shown in Figure 4.8, revealed that 18 out of 21 participants exceeded the statistical threshold for chance performance (58.3%) in all four Motor Task vs. Rest problems. For the remaining three participants, accuracies exceeding chance were obtained for at least two of the Motor Task vs. Rest problems. Across all participants, accuracy ranged from 55.6% to 100.0% (*SD = 12.26%*) in the $\text{Coordination}_{\text{MI}}$ vs. Rest condition, and from 49.8% to 93.7% (*SD = 11.07%*) in the $\text{Control}_{\text{MI}}$ vs. Rest condition. For the ME conditions, accuracy ranged from 55.5% to 99.9% (*SD = 10.44%*) in $\text{Coordination}_{\text{ME}}$ vs. Rest, and from 71.5% to 100.0% (*SD = 7.47%*) in $\text{Control}_{\text{ME}}$ vs. Rest. Notably, 15 out of 21 participants (71.4%) achieved classification accuracies above 70% in the $\text{Coordination}_{\text{MI}}$ vs. Rest condition, while 11 out of 21 participants (52.4%) exceeded this threshold in the $\text{Control}_{\text{MI}}$ vs. Rest condition. For the ME tasks, 19 out of 21 participants (90.5%) surpassed 70% accuracy in $\text{Coordination}_{\text{ME}}$ vs. Rest, and all participants (100%) did so in the $\text{Control}_{\text{ME}}$ vs. Rest condition.

Overall, the Motor Task vs Rest results serve two critical purposes: each motor condition, executed or imagined, generated EEG patterns that were robustly distinguishable from passive rest. This confirms that the control and coordination paradigms elicit neural activity patterns that are measurable by EEG and detectable using our general machine learning pipeline. Consistent, above-chance accuracies across participants and Motor Task vs. Rest classification problems demonstrate that our general classification pipeline functions as intended, with no evidence of implementation errors.

5.3 Interpretation of findings

The combined EEG and TMS findings from this preliminary study support the feasibility of developing MI-based BCI systems for task-specific motor rehabilitation. The observed modulation of CSE and neural activity patterns aligns with prior research in both healthy individuals and neurological populations.

The observation that both $Control_{MI}$ and $Coordination_{MI}$ significantly reduced MEP latency compared to rest, despite no significant MEP amplitude increases, suggests that MI facilitates faster neural conduction without necessarily increasing excitability. This aligns with reports that MI primes the corticospinal tract and enhances signal transmission efficiency even in the absence of muscle contraction [53], [56], [62]. Although amplitude facilitation was not significant at the group level, the observed trends are in line with earlier studies reporting increased MEP amplitudes during MI of hand movements [54]. These findings suggest that MI can engage motor pathways in the absence of movement, reinforcing its potential in neurorehabilitation. The lack of amplitude modulation may reflect individual variability in MI ability [51], [52], or overlapping motor network recruitment across tasks [146], [6]. Such inter-individual variability should be considered when designing BCI-based interventions for clinical populations, including those with MS.

The ability to classify $Control_{MI}$ and $Coordination_{MI}$ with high accuracy confirms that these functions can be decoded from non-invasive EEG signals without overt movement. This reinforces previous findings that mental rehearsal of movement recruits similar neural circuits as actual execution [4], [5], [6], supporting the use of MI as a viable input modality for BCIs designed to support rehabilitation targeting distinct aspects of motor functions, such as coordination or control [8]. Notably, classification accuracies exceeded 80% for both ME and MI conditions using PLV

features, suggesting that these tasks evoke reliably separable cortical signatures, in line with known functional distinctions in motor control and coordination [41], [42].

These results also support previous findings emphasizing the value of functional connectivity in decoding MI tasks [55], [147]. Specifically, PLV, a measure of interregional phase synchronization, outperformed all other feature types, highlighting its strength in capturing complex motor intentions and supporting earlier evidence of its effectiveness in EEG-based network analysis [113].

The highest Motor Task vs. Rest classification accuracies were consistently observed across 5_{fb}, highlighting the frequency-dependent nature of MI-related features. This agrees with foundational work by Pfurtscheller and Lopes [101], who identified *mu* and *beta* band ERD as reliable MI markers. Moreover, classification was best achieved using FBCSP and CORR features, which likely capture broader task-related variance and spatial patterns [111]. FBCSP remains widely adopted for MI decoding of gross motor tasks (e.g., MI vs. rest, or left-hand movement vs. right-hand movement) due to its robustness [112], however, its performance declined when applied to finer control and coordination tasks, supporting the notion that feature selection must align with the complexity of motor representation [121]. Importantly, reducing EEG channels from 64_{ch} to 22_{ch} yielded comparable performance, suggesting the feasibility of more practical BCI implementations. This is consistent with findings by Arvaneh et al. [149], who demonstrated that optimized spatial electrode configurations can preserve essential MI information while reducing system complexity.

The comparable classification accuracy between MI and ME for the Control vs. Coordination task suggests overlapping neural representations. This is encouraging for developing MI-based training

tools aimed at improving specific motor functions, especially for populations like those with MS, where MI has been shown to be decodable despite physical impairments [46].

In summary, this study underscores the importance of aligning feature extraction methods with the specific demands of the decoding objective. PLV shows promise in capturing the distributed synchrony associated with high-level motor planning, while FBCSP remains effective for broader state distinctions, such as Task vs. Rest. These findings support the development of subject-specific BCIs tailored for targeted motor rehabilitation that engage distinct motor functions through task-specific paradigms.

5.4 Comparison with previous findings

While prior MI-based BCI studies have focused on decoding different limbs or simple binary tasks, few have attempted classification within the same effector. Our study targeted two distinct yet functionally meaningful motor components, control and coordination, within the same hand, with direct implications for rehabilitation.

However, classification of fine-grained hand functions (e.g., control vs. coordination) has remained largely unexplored. The few existing studies involving MS participants primarily targeted gross movements such as clenching or tapping and focused on movement vs. rest classification. For example, Shiels et al. [37] and Russo et al. [39] reported decent classification accuracies (>70%) in imagined and executed hand/foot movements in MS, but their tasks lacked functional specificity related to daily motor demands like hand coordination.

To our knowledge, no existing studies have systematically compared MI tasks targeting fine motor control and coordination within the same hand, nor explored their neural separability in the context of neurorehabilitation. In contrast, our work demonstrates that such nuanced MI tasks can evoke

reliably distinct cortical signatures, with classification accuracies exceeding 80% using PLV-based connectivity features.

Moreover, existing MI-based BCI studies in MS have not used TMS to probe neurophysiological changes during MI, limiting insights into corticospinal engagement. For instance, Russo et al. [39], [36] leveraged source-level EEG analysis to enhance classification but did not incorporate physiological validation of cortical engagement via TMS. Carrere et al. [38] demonstrated improvements in gait and earlier ERD onset following an 8-week BCI-FES intervention, but their work focused exclusively on lower-limb rehabilitation, making it less relevant to upper-limb fine motor control.

Our study is thus the first to integrate TMS and EEG to decode fine motor functions (control vs. coordination), offering converging evidence of preserved and differentiable motor network engagement during MI. This is especially relevant for MS, where motor impairments often affect dexterous control.

Importantly, none of the reviewed MS-based BCI studies employed FBCSP or connectivity features like PLV. Nor did they systematically evaluate feature extraction or classification pipelines for optimal MI decoding. In contrast, our approach highlights how task design, feature selection, and classifier tuning can substantially improve decoding of fine motor intentions in both ME and MI conditions.

In summary, thesis study makes several novel contributions:

- It is the first to classify coordination vs. control MI tasks using EEG.
- It introduces a dual-modality approach (TMS/EMG + EEG) to assess motor pathway activation during MI, which is absent in prior MS-based BCI studies.

- It employs functional connectivity measures and compares multiple feature extraction and classification methods, demonstrating their utility in decoding nuanced hand functions.

These innovations lay the groundwork for the development of more personalized MI-based BCI systems aimed at supporting hand rehabilitation in MS.

Chapter 6 Conclusion

6.1 Conclusion

This study investigated whether MI tasks targeting motor control and coordination modulate CSE, and whether these two forms of motor intention can be reliably distinguished using EEG. Using TMS-evoked MEPs, we found that ME tasks significantly increased MEP amplitudes and reduced latencies compared to rest, confirming enhanced CSE and faster corticospinal conduction during voluntary movement. While MI tasks did not significantly increase MEP amplitude, they did lead to reduced latency, suggesting that MI may facilitate signal transmission even without overt movement. This finding aligns with prior evidence that MI primes the motor system, enhancing conduction efficiency despite limited excitability changes.

However, no significant physiological differences were observed between the control and coordination variants within either MI or ME tasks. This lack of MEP amplitude differentiation may be due to overlapping motor network recruitment, insufficient MI task complexity, or variability in individual imagery ability. Notably, while these subtleties were not evident in MEP measures, EEG-based classification revealed a contrasting outcome.

Crucially, EEG-based analyses revealed that $\text{Control}_{\text{MI}}$ and $\text{Coordination}_{\text{MI}}$ could be reliably distinguished on a single-trial basis, with classification accuracies (~80%) significantly above chance in most participants. These results suggest that control and coordination are encoded by distinct neural processes, consistently represented during both imagined and executed movements. Among the feature types tested, phase-based connectivity (PLV) outperformed others, highlighting the value of inter-regional synchrony in capturing complex motor representations.

Collectively, these findings underscore the importance of tailoring feature extraction methods to the specific decoding objective. They also support the development of MI-based BCIs designed to target distinct motor functions like control and coordination.

6.1 Limitations and future work

While the findings of this study are promising, several limitations should be acknowledged:

- This study involved a small group of healthy participants, which limits the generalizability of the results to clinical populations, particularly individuals with MS. Given that MS-related neural alterations may affect EEG patterns, CSE, and response to MI, future research should recruit participants from the target population to validate the neural separability of control and coordination tasks. It is also essential to determine whether functional connectivity features, such as PLV, which demonstrated strong performance in differentiating $Control_{MI}$ and $Coordination_{MI}$, remain stable and effective across sessions and under varying task demands. Considering the common impairment of fine motor functions in MS, especially hand coordination and control, confirming these neural distinctions in clinical populations is a critical step toward developing effective rehabilitation-oriented BCIs. Furthermore, subsequent studies should evaluate whether MI-based BCI interventions can produce measurable improvements in hand motor function using standardized clinical assessments. To support this translational goal, personalized and adaptive classification algorithms capable of accommodating evolving neural profiles in MS patients will be necessary.

- Although the tasks were designed to represent motor control and coordination, other influential variables, such as mental workload, motivation, and task complexity, were not systematically assessed. It is possible that some other aspects of the tasks, apart from the

underlying motor functions of control and coordination, could have contributed to the observed results. Future research should control for these factors to isolate the neural correlates of motor coordination and control more definitively.

- No EMG recording was performed during EEG data acquisition, raising the possibility that subtle or unintended muscle activations may have confounded MI classification. Incorporating simultaneous EMG monitoring in future studies would help rule out these artifacts and validate the purity of MI signals.
- The current study was conducted offline in a controlled environment. It is not yet clear how these findings will generalize to online or real-time BCI applications. Future work should implement and test the proposed pipelines in real-time BCI environments to assess their practical viability and responsiveness.
- Real-world BCI systems include real-time feedback, which has been shown to improve user engagement and classification accuracy. The current study did not incorporate such feedback. Future experiments should integrate user feedback loops to enhance learning, motivation, and performance.
- The study did not collect participant feedback regarding the perceived difficulty or clarity of the MI tasks. Understanding user perception and evaluating how these tasks are experienced over time is crucial for improving the long-term usability and acceptability of BCI systems. Future work should include qualitative measures to assess task engagement, comfort, and cognitive load. Additionally, integrating feedback from patients, therapists, and clinicians will be essential for designing BCI systems that are not only effective but also user-friendly, sustainable, and tailored to real-world rehabilitation needs.

Bibliography and references

[1] M. A. Khan, R. Das, H. K. Iversen, and S. Puthusserypady, “Review on motor imagery based BCI systems for upper limb post-stroke neurorehabilitation: From designing to application,” *Comput Biol Med*, vol. 123, p. 103843, 2020, doi: 10.1016/j.compbiomed.2020.103843.

[2] R. Bertoni, I. Lamers, C. C. Chen, P. Feys, and D. Cattaneo, “Unilateral and bilateral upper limb dysfunction at body functions, activity and participation levels in people with multiple sclerosis,” *Multiple Sclerosis*, vol. 21, no. 12, pp. 1566–1574, 2015, doi: 10.1177/1352458514567553.

[3] J. J. Daly and J. R. Wolpaw, “Brain-computer interfaces in neurological rehabilitation,” *Lancet Neurol*, vol. 7, pp. 1032–1043, 2008, doi: 10.1016/S1474.

[4] P. Dechent, K. D. Merboldt, and J. Frahm, “Is the human primary motor cortex involved in motor imagery?,” *Cognitive Brain Research*, vol. 19, no. 2, pp. 138–144, Apr. 2004, doi: 10.1016/j.cogbrainres.2003.11.012.

[5] J. Decety, “The neurophysiological basis of motor imagery,” 1996.

[6] M. Lotze and U. Halsband, “Motor imagery,” *J Physiol Paris*, vol. 99, no. 4–6, pp. 386–395, Jun. 2006, doi: 10.1016/j.jphysparis.2006.03.012.

[7] F. Lotte, L. Bougrain, and M. Clerc, “Electroencephalography (EEG)-based Brain-Computer Interfaces,” *Wiley Encyclopedia of Electrical and Electronics Engineering*, p. 44, 2015, doi: 10.1002/047134608X.W8278.

[8] L. Brusini, F. Stival, F. Setti, E. Menegatti, G. Menegaz, and S. F. Storti, “A Systematic Review on Motor-Imagery Brain-Connectivity-Based Computer Interfaces,” *IEEE Trans Hum Mach Syst*, vol. 51, no. 6, pp. 725–733, Dec. 2021, doi: 10.1109/THMS.2021.3115094.

[9] J. R. Wolpaw, D. J. Mcfarland, G. W. Neat, and C. A. Forneris, “An EEG-based brain-computer interface for cursor control,” *Electroencephalogr Clin Neurophysiol*, vol. 78, pp. 252–259, 1991.

[10] L. Farwell and E. Donchin, “Talking off the top of your head: toward a mental prosthesis utilizing event-related brain potentials,” *Electroencephalogr Clin Neurophysiol*, vol. 70, pp. 510–523, 1988.

[11] F. D. K. J. Pfurtscheller G, “Brain-Computer Interface—a new communication device for handicapped persons,” *Journal of Microcomputer Applications*, vol. 16, no. 3, pp. 293–299, 1993.

[12] T. J. H. Bovend’eerdt, H. Dawes, C. Sackley, and D. T. Wade, “Practical research-based guidance for motor imagery practice in neurorehabilitation,” *Disabil Rehabil*, vol. 34, no. 25, pp. 2192–2200, Dec. 2012, doi: 10.3109/09638288.2012.676703.

[13] K. K. Ang and C. Guan, “Brain-computer interface for neurorehabilitation of upper limb after stroke,” *Proceedings of the IEEE*, vol. 103, no. 6, pp. 944–953, Jun. 2015, doi: 10.1109/JPROC.2015.2415800.

[14] K. K. Ang *et al.*, “Clinical study of neurorehabilitation in stroke using EEG-based motor imagery brain-computer interface with robotic feedback,” *2010 Annual International Conference of the IEEE Engineering in Medicine and Biology Society, EMBC’10*, pp. 5549–5552, 2010, doi: 10.1109/IEMBS.2010.5626782.

[15] M. A. Cervera *et al.*, “Brain-computer interfaces for post-stroke motor rehabilitation: a meta-analysis,” May 01, 2018, *Wiley-Blackwell*. doi: 10.1002/acn3.544.

[16] T. Ono *et al.*, “Brain-computer interface with somatosensory feedback improves functional recovery from severe hemiplegia due to chronic stroke,” *Front Neuroeng*, vol. 7, Jul. 2014, doi: 10.3389/fneng.2014.00019.

[17] S. Yang *et al.*, “Exploring the Use of Brain-Computer Interfaces in Stroke Neurorehabilitation,” *Biomed Res Int*, vol. 2021, 2021, doi: 10.1155/2021/9967348.

[18] Y. Qin *et al.*, “Brain-computer interface training for motor recovery after stroke,” Jun. 09, 2022, *John Wiley and Sons Ltd*. doi: 10.1002/14651858.CD015065.

[19] A. Zimmermann-Schlatter, C. Schuster, M. A. Puhan, E. Siekierka, and J. Steurer, “Efficacy of motor imagery in post-stroke rehabilitation: A systematic review,” *J Neuroeng Rehabil*, vol. 5, 2008, doi: 10.1186/1743-0003-5-8.

[20] Y. Tong *et al.*, “Motor imagery-based rehabilitation: Potential neural correlates and clinical application for functional recovery of motor deficits after stroke,” 2017, *International Society on Aging and Disease*. doi: 10.14336/AD.2016.1012.

[21] M. D. , Ph. D. , C. F. L. M. D. , and P. A. C. M. D. Daniel S. Reich, “Multiple Sclerosis,” *N Engl J Med*, pp. 169–180, 2018, doi: 10.1056/NEJMra1401483.

[22] F. D. Lublin *et al.*, “How patients with multiple sclerosis acquire disability,” *Brain*, vol. 145, no. 9, pp. 3147–3161, Sep. 2022, doi: 10.1093/brain/awac016.

[23] I. Lamers and P. Feys, “Assessing upper limb function in multiple sclerosis,” *Multiple Sclerosis Journal*, vol. 20, no. 7, pp. 775–784, 2014, doi: 10.1177/1352458514525677.

[24] L. Pellegrino, M. Coscia, M. Muller, C. Solaro, and M. Casadio, “Evaluating upper limb impairments in multiple sclerosis by exposure to different mechanical environments,” *Sci Rep*, vol. 8, no. 1, Dec. 2018, doi: 10.1038/s41598-018-20343-y.

[25] N. Valè *et al.*, “Characterization of Upper Limb Impairments at Body Function, Activity, and Participation in Persons With Multiple Sclerosis by Behavioral and EMG Assessment: A Cross-Sectional Study,” *Front Neurol*, vol. 10, Feb. 2020, doi: 10.3389/fneur.2019.01395.

[26] I. Lipp and V. Tomassini, “Neuroplasticity and motor rehabilitation in multiple sclerosis,” *Front Neurol*, vol. 6, no. MAR, 2015, doi: 10.3389/fneur.2015.00059.

[27] E. Tavazzi *et al.*, “Neuroplasticity and Motor Rehabilitation in Multiple Sclerosis: A Systematic Review on MRI Markers of Functional and Structural Changes,” Oct. 06, 2021, *Frontiers Media S.A.* doi: 10.3389/fnins.2021.707675.

[28] L. Prosperini and M. Di Filippo, “Beyond clinical changes: Rehabilitation-induced neuroplasticity in MS,” *Multiple Sclerosis Journal*, vol. 25, no. 10, pp. 1348–1362, 2019, doi: 10.1177/1352458519846096.

[29] E. Heremans *et al.*, “Cued motor imagery in patients with multiple sclerosis,” *Neuroscience*, vol. 206, pp. 115–121, 2012, doi: 10.1016/j.neuroscience.2011.12.060.

[30] D. Benito-Villalvilla, I. L. De Uralde-Villanueva, M. Ríos-León, Á. C. Álvarez-Melcón, and P. Martín-Casas, “Effectiveness of motor imagery in patients with multiple sclerosis: A systematic review,” *Rev Neurol*, vol. 72, no. 5, pp. 157–167, 2021, doi: 10.33588/RN.7205.2020436.

[31] B. Seebacher, R. Kuisma, A. Glynn, and T. Berger, “Effects and mechanisms of differently cued and non-cued motor imagery in people with multiple sclerosis: A randomised controlled trial,” *Multiple Sclerosis Journal*, vol. 25, no. 12, pp. 1593–1604, 2019, doi: 10.1177/1352458518795332.

[32] A. Tacchino *et al.*, “Motor imagery has a priming effect on motor execution in people with multiple sclerosis,” *Front Hum Neurosci*, vol. 17, Sep. 2023, doi: 10.3389/fnhum.2023.1179789.

[33] M. Hanson and M. Concialdi, “Motor imagery in multiple sclerosis: exploring applications in therapeutic treatment,” *J Neurophysiol*, vol. 121, pp. 347–349, 2019, doi: 10.1152/jn.00291.2018.-Motor.

[34] A. Tacchino *et al.*, “Motor imagery as a function of disease severity in multiple sclerosis: An fMRI study,” *Front Hum Neurosci*, vol. 11, Jan. 2018, doi: 10.3389/fnhum.2017.00628.

[35] A. Singh, P. Zamboni, and M. Khare, “Prospect of brain-machine interface in motor disabilities: The future support for multiple sclerosis patient to improve quality of life,” *Ann Med Health Sci Res*, vol. 4, no. 3, p. 305, 2014, doi: 10.4103/2141-9248.133447.

[36] M. C. M. S. T. A. S. C.-H. S. L. S. E. J. D. B. G. John S Russo, “Feasibility of Using Source-Level Brain Computer Interface for People with Multiple Sclerosis,” Aug. 2021, doi: 10.1109/EMBC40787.2023.10340364.

[37] T. A. Shiels *et al.*, “Feasibility of using discrete Brain Computer Interface for people with Multiple Sclerosis,” in *Proceedings of the Annual International Conference of the IEEE Engineering in Medicine and Biology Society, EMBS*, Institute of Electrical and Electronics Engineers Inc., 2021, pp. 5686–5689. doi: 10.1109/EMBC46164.2021.9629518.

[38] L. Carolina Carrere, M. Taborda, C. Ballario, and C. Tabernig, “Effects of brain-computer interface with functional electrical stimulation for gait rehabilitation in multiple sclerosis patients: Preliminary findings in gait speed and event-related desynchronization onset latency,” *J Neural Eng*, vol. 18, no. 6, Dec. 2021, doi: 10.1088/1741-2552/ac39b8.

[39] J. S. Russo, T. A. Shiels, C.-H. S. Lin, S. E. John, and D. B. Grayden, “Feasibility of source-level motor imagery classification for people with multiple sclerosis,” *J Neural Eng*, vol. 22, no. 2, p. 026020, Apr. 2025, doi: 10.1088/1741-2552/adbec1.

[40] M. Kolmos, M. Munoz-Novoa, K. Sunnerhagen, M. A. Murphy, and C. Kruuse, “Upper-extremity motor recovery after stroke: A systematic review and meta-analysis of usual care in trials and observational studies,” Jan. 15, 2025, *Elsevier B.V.* doi: 10.1016/j.jns.2024.123341.

[41] A. , & W. M. H. Shumway-Cook, “Motor Control: Translating Research Into Clinical Practice, 5th Edition.,” 2022.

[42] S. P. Swinnen, “Intermanual coordination: From behavioural principles to neural-network interactions,” May 2002. doi: 10.1038/nrn807.

[43] E. J. Brouwer, M. Strik, E. J. Brouwer, M. Strik, M. Strik, and M. M. Schoonheim, “The role of the cerebellum in multiple sclerosis: structural damage and disconnecting networks,” Oct. 01, 2024, *Elsevier Ltd*. doi: 10.1016/j.cobeha.2024.101436.

[44] M. Strik *et al.*, “Axonal loss in major sensorimotor tracts is associated with impaired motor performance in minimally disabled multiple sclerosis patients,” *Brain Commun*, vol. 3, no. 2, 2021, doi: 10.1093/braincomms/fcab032.

[45] M. Daams *et al.*, “Unraveling the neuroimaging predictors for motor dysfunction in long-standing multiple sclerosis,” 2015. [Online]. Available: http://www.fmrib.ox.ac.

[46] J. S. Russo, T. A. Shiels, C. H. S. Lin, S. E. John, and D. B. Grayden, “Decoding imagined movement in people with multiple sclerosis for brain-computer interface translation,” *J Neural Eng*, vol. 22, no. 1, Feb. 2025, doi: 10.1088/1741-2552/adaa1d.

[47] A. M. Joshua, “Neuroplasticity,” in *Physiotherapy for Adult Neurological Conditions.* , A. M. Joshua, Ed., Springer, Singapore., 2022, pp. 1–30. Accessed: Dec. 11, 2024. [Online]. Available: https://doi.org/10.1007/978-981-19-0209-3_1

[48] P. M. Rossini, M. Ada, N. Ferilli, and F. Ferreri, “Cortical plasticity and brain computer interface,” 2012. [Online]. Available: https://www.researchgate.net/publication/225054051

[49] A. M. Ladda, F. Lebon, and M. Lotze, “Using motor imagery practice for improving motor performance – A review,” *Brain Cogn*, vol. 150, Jun. 2021, doi: 10.1016/j.bandc.2021.105705.

[50] F. Malouin, C. L. Richards, P. L. Jackson, M. F. Lafleur, A. Durand, and J. Doyon, “The kinesthetic and visual imagery questionnaire (KVIQ) for assessing motor imagery in persons with physical disabilities: A reliability and construct validity study,” *Journal of Neurologic Physical Therapy*, vol. 31, no. 1, pp. 20–29, 2007, doi: 10.1097/01.NPT.0000260567.24122.64.

[51] J. Williams, A. J. Pearce, M. Loporto, T. Morris, and P. S. Holmes, “The relationship between corticospinal excitability during motor imagery and motor imagery ability,” *Behavioural Brain Research*, vol. 226, no. 2, pp. 369–375, Jan. 2012, doi: 10.1016/j.bbr.2011.09.014.

[52] F. Lebon, W. D. Byblow, C. Collet, A. Guillot, and C. M. Stinear, “The modulation of motor cortex excitability during motor imagery depends on imagery quality,” *European Journal of Neuroscience*, vol. 35, no. 2, pp. 323–331, Jan. 2012, doi: 10.1111/j.1460-9568.2011.07938.x.

[53] S. Grosprêtre, C. Ruffino, and F. Lebon, “Motor imagery and cortico-spinal excitability: A review,” *Eur J Sport Sci*, vol. 16, no. 3, pp. 317–324, 2016, doi: 10.1080/17461391.2015.1024756.

[54] K. M. R. Foysal and S. N. Baker, “Induction of plasticity in the human motor system by motor imagery and transcranial magnetic stimulation,” *Journal of Physiology*, vol. 598, no. 12, pp. 2385–2396, Jun. 2020, doi: 10.1113/JP279794.

[55] L. Xu *et al.*, “Motor execution and motor imagery: A comparison of functional connectivity patterns based on graph theory,” *Neuroscience*, vol. 261, pp. 184–194, Mar. 2014, doi: 10.1016/j.neuroscience.2013.12.005.

[56] T. Kasai, S. Kawai, M. Kawanishi, and S. Yahagi, “Ž. Evidence for facilitation of motor evoked potentials MEPs induced by motor imagery,” 1997.

[57] P. M. Rossini *et al.*, “Non-invasive electrical and magnetic stimulation of the brain, spinal cord, roots and peripheral nerves: Basic principles and procedures for routine clinical and research application: An updated report from an I.F.C.N. Committee,” Jun. 01, 2015, *Elsevier Ireland Ltd*. doi: 10.1016/j.clinph.2015.02.001.

[58] J. Lefaucheur, “Transcranial magnetic stimulation ,” in *In Handbook of Clinical Neurology*, vol. 160, Elsevier Health Sciences, 2019, pp. 559–580.

[59] B. Moezzi *et al.*, “Simulation of electromyographic recordings following transcranial magnetic stimulation,” *J Neurophysiol*, vol. 120, pp. 2532–2541, 2018, doi: 10.1152/jn.00626.2017.-Transcranial.

[60] W. Liang, Y. Xu, J. Schmidt, L. Zhang, and K. L. Ruddy, “Upregulating excitability of corticospinal pathways in stroke patients using TMS neurofeedback; A pilot study,” *Neuroimage Clin*, vol. 28, 2020, doi: 10.1016/j.nicl.2020.102465.

[61] C. M. Stinear, W. D. Byblow, M. Steyvers, O. Levin, and S. P. Swinnen, “Kinesthetic, but not visual, motor imagery modulates corticomotor excitability,” *Exp Brain Res*, vol. 168, no. 1–2, pp. 157–164, Jan. 2006, doi: 10.1007/s00221-005-0078-y.

[62] F. Kaneko, T. Hayami, T. Aoyama, and T. Kizuka, “Motor imagery and electrical stimulation reproduce corticospinal excitability at levels similar to voluntary muscle contraction,” *J Neuroeng Rehabil*, vol. 11, no. 1, Jun. 2014, doi: 10.1186/1743-0003-11-94.

[63] S. Irie, T. Nakajima, S. Suzuki, R. Ariyasu, T. Komiyama, and Y. Ohki, “Motor imagery enhances corticospinal transmission mediated by cervical premotoneurons in humans,” *J Neurophysiol*, vol. 124, pp. 86–101, 2020, doi: 10.1152/jn.00574.2019.-Motor.

[64] E. Yoxon and T. N. Welsh, “Motor system activation during motor imagery is positively related to the magnitude of cortical plastic changes following motor imagery training,” *Behavioural Brain Research*, vol. 390, Jul. 2020, doi: 10.1016/j.bbr.2020.112685.

[65] J. Šoda, S. Pavelin, I. Vujović, and M. Rogić Vidaković, “Assessment of Motor Evoked Potentials in Multiple Sclerosis,” Jan. 01, 2023, *MDPI*. doi: 10.3390/s23010497.

[66] C. Neuper and G. Pfurtscheller, “Neurofeedback Training for BCI Control,” in *Frontiers Collection*, vol. Part F952, Springer VS, 2009, pp. 65–78. doi: 10.1007/978-3-642-02091-9_4.

[67] C. Ruffino, C. Papaxanthis, and F. Lebon, “Neural plasticity during motor learning with motor imagery practice: Review and perspectives,” Jan. 26, 2017, *Elsevier Ltd*. doi: 10.1016/j.neuroscience.2016.11.023.

[68] F. G. G. , L. R. , D. J. E. Bermúdez i Badia S., *Virtual reality for Sensorimotor rehabilitation post stroke: design principles and evidence in Neurorehabilitation Technology*. Springer International Publishing, 2016.

[69] C. Marquez-Chin and M. R. Popovic, “Functional electrical stimulation therapy for restoration of motor function after spinal cord injury and stroke: A review,” May 24, 2020, *BioMed Central Ltd.* doi: 10.1186/s12938-020-00773-4.

[70] J. M. Veerbeek, A. C. Langbroek-Amersfoort, E. E. H. Van Wegen, C. G. M. Meskers, and G. Kwakkel, “Effects of Robot-Assisted Therapy for the Upper Limb after Stroke,” Feb. 01, 2017, *SAGE Publications Inc.* doi: 10.1177/1545968316666957.

[71] C. A. Stefano Filho *et al.*, “On the (in)efficacy of motor imagery training without feedback and event-related desynchronizations considerations,” *Biomed Phys Eng Express*, vol. 6, no. 3, May 2020, doi: 10.1088/2057-1976/ab8992.

[72] M. S. Kim *et al.*, “Efficacy of brain-computer interface training with motor imagery-contingent feedback in improving upper limb function and neuroplasticity among persons with chronic stroke: a double-blinded, parallel-group, randomized controlled trial,” *J Neuroeng Rehabil*, vol. 22, no. 1, Dec. 2025, doi: 10.1186/s12984-024-01535-2.

[73] A. Kruse, Z. Suica, J. Taeymans, and C. Schuster-Amft, “Effect of brain-computer interface training based on non-invasive electroencephalography using motor imagery on functional recovery after stroke - a systematic review and meta-analysis,” *BMC Neurol*, vol. 20, no. 1, Dec. 2020, doi: 10.1186/s12883-020-01960-5.

[74] J. Liu *et al.*, “Efficacy and safety of brain–computer interface for stroke rehabilitation: an overview of systematic review,” *Front Hum Neurosci*, vol. 19, Mar. 2025, doi: 10.3389/fnhum.2025.1525293.

[75] W. J. Brownlee, T. A. Hardy, F. Fazekas, and D. H. Miller, “Diagnosis of multiple sclerosis: progress and challenges,” Apr. 01, 2017, *Lancet Publishing Group*. doi: 10.1016/S0140-6736(16)30959-X.

[76] L. Messinis, P. Papathanasopoulos, M. H. Kosmidis, G. Nasios, and M. Kambanaros, "Neuropsychological Features of Multiple Sclerosis: Impact and Rehabilitation," *Behavioural Neurology*, vol. 2018, 2018, doi: 10.1155/2018/4831647.

[77] F. Khan, L. Turner-Stokes, L. Ng, and T. Kilpatrick, "Multidisciplinary rehabilitation for adults with multiple sclerosis," 2007, *John Wiley and Sons Ltd*. doi: 10.1002/14651858.CD006036.pub2.

[78] B. Amatya, F. Khan, and M. Galea, "Rehabilitation for people with multiple sclerosis: An overview of Cochrane Reviews," Jan. 14, 2019, *John Wiley and Sons Ltd*. doi: 10.1002/14651858.CD012732.pub2.

[79] G. H. Kraft *et al.*, "Assessment of upper extremity function in multiple sclerosis: Review and opinion," *Postgrad Med*, vol. 126, no. 5, pp. 102–108, Jan. 2014, doi: 10.3810/pgm.2014.09.2803.

[80] B.-O. A. P. F. P. P. S. A. V. S. R. MA. Filippi M, "Multiple sclerosis," *Nat Rev Dis Primers.* , vol. 4, no. 1, p. 43, Nov. 2018.

[81] P. , B. J. , & K. G. Langhorne, *Stroke rehabilitation*, vol. 377(9778). The Lancet, 2011.

[82] D. Pinter *et al.*, "MRI correlates of cognitive improvement after home-based EEG neurofeedback training in patients with multiple sclerosis: a pilot study," *J Neurol*, vol. 268, no. 10, pp. 3808–3816, Oct. 2021, doi: 10.1007/s00415-021-10530-9.

[83] B. Seebacher, R. Kuisma, A. Glynn, and T. Berger, "The effect of rhythmic-cued motor imagery on walking, fatigue and quality of life in people with multiple sclerosis: A randomised controlled trial," *Multiple Sclerosis*, vol. 23, no. 2, pp. 286–296, Feb. 2017, doi: 10.1177/1352458516644058.

[84] Y. M. Tabrizi, S. Mazhari, M. A. Nazari, N. Zangiabadi, V. Sheibani, and S. Azarang, "Compromised motor imagery ability in individuals with multiple sclerosis and mild physical disability: An ERP study," *Clin Neurol Neurosurg*, vol. 115, no. 9, pp. 1738–1744, 2013, doi: 10.1016/j.clineuro.2013.04.002.

[85] E. Villa-Berges *et al.*, "Motor Imagery and Mental Practice in the Subacute and Chronic Phases in Upper Limb Rehabilitation after Stroke: A Systematic Review," 2023, *Hindawi Limited*. doi: 10.1155/2023/3752889.

[86] P. Feys *et al.*, "The Nine-Hole Peg Test as a manual dexterity performance measure for multiple sclerosis," Apr. 01, 2017, *SAGE Publications Ltd*. doi: 10.1177/1352458517690824.

[87] T. J. Bradberry, R. J. Gentili, and J. L. Contreras-Vidal, "Fast attainment of computer cursor control with noninvasively acquired brain signals," *J Neural Eng*, vol. 8, no. 3, Jun. 2011, doi: 10.1088/1741-2560/8/3/036010.

[88] J. Lee, N. Mukae, J. Arata, K. Iihara, and M. Hashizume, "Comparison of feature vector compositions to enhance the performance of NIRS-BCI-triggered robotic hand orthosis for post-stroke motor recovery," *Applied Sciences (Switzerland)*, vol. 9, no. 18, Sep. 2019, doi: 10.3390/app9183845.

[89] Y. , L. S. , & L. D. Lee, “Wearable Haptic Device for Stiffness Rendering of Virtual Objects in Augmented Reality. Figure 1. ,” *Applied Sciences*, vol. 11, no. 15, p. 6932, 2021.

[90] M. A. , T. K. , & A.-F. A. Gull, “A 4-DOF upper-limb exoskeleton for physical human-robot interaction: Design, control, and evaluation.,” *Applied Sciences*, vol. 11, no. 13, p. 5865, 2021.

[91] A. Cuesta-Gómez, F. Molina-Rueda, M. Carratala-Tejada, E. Imatz-Ojanguren, D. Torricelli, and J. C. Miangolarra-Page, “The use of functional electrical stimulation on the upper limb and interscapular muscles of patients with stroke for the improvement of reaching movements: A feasibility study,” *Front Neurol*, vol. 8, no. MAY, May 2017, doi: 10.3389/fneur.2017.00186.

[92] U. Salahuddin and P. X. Gao, “Signal Generation, Acquisition, and Processing in Brain Machine Interfaces: A Unified Review,” Sep. 13, 2021, *Frontiers Media S.A.* doi: 10.3389/fnins.2021.728178.

[93] D. J. McFarland and J. R. Wolpaw, “EEG-based brain–computer interfaces,” Dec. 01, 2017, *Elsevier B.V.* doi: 10.1016/j.cobme.2017.11.004.

[94] D. Rathee, H. Raza, S. Roy, and G. Prasad, “A magnetoencephalography dataset for motor and cognitive imagery-based brain-computer interface,” *Sci Data*, vol. 8, no. 1, Dec. 2021, doi: 10.1038/s41597-021-00899-7.

[95] B. Sorger and R. Goebel, “Chapter 21 - Real-time fMRI for brain-computer interfacing,” in *Brain-Computer Interfaces*, vol. 168, N. F. Ramsey and J. del R. Millán, Eds., in Handbook of Clinical Neurology, vol. 168. , Elsevier, 2020, pp. 289–302. doi: https://doi.org/10.1016/B978-0-444-63934-9.00021-4.

[96] N. Naseer and K. S. Hong, “fNIRS-based brain-computer interfaces: A review,” Jan. 28, 2015, *Frontiers Media S. A.* doi: 10.3389/fnhum.2015.00003.

[97] X. Y. Liu *et al.*, “Recent applications of EEG-based brain-computer-interface in the medical field,” Dec. 01, 2025, *BioMed Central Ltd*. doi: 10.1186/s40779-025-00598-z.

[98] G. Schalk and E. C. Leuthardt, “Brain-Computer Interfaces Using Electrocorticographic Signals,” *IEEE Rev Biomed Eng*, vol. 4, pp. 140–154, 2011, doi: 10.1109/RBME.2011.2172408.

[99] L. Meyer-Baese, H. Watters, and S. Keilholz, “Spatiotemporal patterns of spontaneous brain activity: a mini-review,” *Neurophotonics*, vol. 9, no. 03, Apr. 2022, doi: 10.1117/1.nph.9.3.032209.

[100] Y. Jeon, C. S. Nam, Y. J. Kim, and M. C. Whang, “Event-related (De)synchronization (ERD/ERS) during motor imagery tasks: Implications for brain-computer interfaces,” *Int J Ind Ergon*, vol. 41, no. 5, pp. 428–436, Sep. 2011, doi: 10.1016/j.ergon.2011.03.005.

[101] G. Pfurtscheller and F. H. Lopes Da Silva, “Invited review Event-related EEG/MEG synchronization and desynchronization: basic principles,” 1999. doi: 10.1016/s1388-2457(99)00141-8.

[102] L. H. J. H. E. C. Klem GH, “The ten-twenty electrode system of the International Federation ,” *The International Federation of Clinical Neurophysiology. Electroencephalogr Clin Neurophysiol Suppl.* , vol. 52, pp. 3–6, 1999.

[103] “EEG Electrode Positions in the 10-10 System. Wikimedia Commons, https://commons.wikimedia.org/wiki/File:EEG_10-10_system_with_additional_information.svg. Accessed July 2025.”

[104] A. Widmann, E. Schröger, and B. Maess, “Digital filter design for electrophysiological data - a practical approach,” *J Neurosci Methods*, vol. 250, pp. 34–46, Jul. 2015, doi: 10.1016/j.jneumeth.2014.08.002.

[105] D. J. Mcfarland, L. M. Mccane, S. V David, and J. R. Wolpaw, “Spatial filter selection for EEG-based communication,” 1997.

[106] A. Rajalakshmi and S. S. Sridhar, “A Study of Time Domain Features of EEG Signal Analysis.”

[107] O. Dressler, G. Schneider, G. Stockmanns, and E. F. Kochs, “Awareness and the EEG power spectrum: Analysis of frequencies,” *Br J Anaesth*, vol. 93, no. 6, pp. 806–809, 2004, doi: 10.1093/bja/aeh270.

[108] S. Morales and M. E. Bowers, “Time-frequency analysis methods and their application in developmental EEG data,” *Dev Cogn Neurosci*, vol. 54, Apr. 2022, doi: 10.1016/j.dcn.2022.101067.

[109] Z. J. Kales, M. S. Lazar, and S. Z. Zhou, “Spatial Patterns Underlying Population Differences in the Background EEG,” 1990.

[110] M. Grosse-Wentrup and M. Buss, “Multiclass common spatial patterns and information theoretic feature extraction,” *IEEE Trans Biomed Eng*, vol. 55, no. 8, pp. 1991–2000, Aug. 2008, doi: 10.1109/TBME.2008.921154.

[111] B. Blankertz, R. Tomioka, S. Lemm, M. Kawanabe, and K.-R. Müller, “Optimizing Spatial Filters for Robust EEG Single-Trial Analysis,” 2008.

[112] K. K. Ang, Z. Y. Chin, C. Wang, C. Guan, and H. Zhang, “Filter bank common spatial pattern algorithm on BCI competition IV datasets 2a and 2b,” *Front Neurosci*, no. MAR, 2012, doi: 10.3389/fnins.2012.00039.

[113] M. Hassan, O. Dufor, I. Merlet, C. Berrou, and F. Wendling, “EEG source connectivity analysis: From dense array recordings to brain networks,” *PLoS One*, vol. 9, no. 8, Aug. 2014, doi: 10.1371/journal.pone.0105041.

[114] K. J. Friston, “Functional and Effective Connectivity: A Review,” *Brain Connect*, vol. 1, no. 1, pp. 13–36, 2011, doi: 10.1089/brain.2011.0008.

[115] G. Chiarion, L. Sparacino, Y. Antonacci, L. Faes, and L. Mesin, “Connectivity Analysis in EEG Data: A Tutorial Review of the State of the Art and Emerging Trends,” Mar. 01, 2023, *MDPI*. doi: 10.3390/bioengineering10030372.

[116] C. Ding and H. Peng, “Minimum Redundancy Feature Selection from Microarray Gene Expression Data,” 2003.

[117] R. A. FISHER, “THE USE OF MULTIPLE MEASUREMENTS IN TAXONOMIC PROBLEMS,” *Ann Eugen*, vol. 7, no. 2, pp. 179–188, Sep. 1936, doi: 10.1111/j.1469-1809.1936.tb02137.x.

[118] “K Fukunaga. Introduction to Statistical pattern recognition. Academic Press Inc, 1990.”.

[119] “G James. An introduction to statistical learning. California: Springer, 2013.”.

[120] “Jerome H Friedman. \Regularized Discriminant Analysis". In: J. Am. Stat. As- soc. 84.405 (1989), p. 165.”

[121] F. Lotte *et al.*, “A review of classification algorithms for EEG-based brain-computer interfaces: A 10 year update,” Apr. 16, 2018, *Institute of Physics Publishing*. doi: 10.1088/1741-2552/aab2f2.

[122] C. Cortes, V. Vapnik, and L. Saitta, “Support-Vector Networks Editor,” Kluwer Academic Publishers, 1995.

[123] W. Wu, X. Gao, B. Hong, and S. Gao, “Classifying single-trial EEG during motor imagery by iterative spatio-spectral patterns learning (ISSPL),” *IEEE Trans Biomed Eng*, vol. 55, no. 6, pp. 1733–1743, Jun. 2008, doi: 10.1109/TBME.2008.919125.

[124] P. Ghane, N. Z. Naghsh, and U. Braga-Neto, “Comparison of Classification Algorithms Towards Subject-Specific and Subject-Independent BCI,” Jan. 2021, [Online]. Available: http://arxiv.org/abs/2012.12473

[125] Z. Cao, “A review of artificial intelligence for EEG-based brain–computer interfaces and applications,” *Brain Science Advances*, vol. 6, no. 3, pp. 162–170, Sep. 2020, doi: 10.26599/bsa.2020.9050017.

[126] J. R. Quinlan, “Induction of Decision Trees,” 1986.

[127] S. Guan, K. Zhao, and S. Yang, “Motor Imagery EEG Classification Based on Decision Tree Framework and Riemannian Geometry,” *Comput Intell Neurosci*, vol. 2019, 2019, doi: 10.1155/2019/5627156.

[128] R. Fu, Y. Tian, T. Bao, Z. Meng, and P. Shi, “Improvement Motor Imagery EEG Classification Based on Regularized Linear Discriminant Analysis,” *J Med Syst*, vol. 43, no. 6, Jun. 2019, doi: 10.1007/s10916-019-1270-0.

[129] Y. Roy, H. Banville, I. Albuquerque, A. Gramfort, T. H. Falk, and J. Faubert, “Deep learning-based electroencephalography analysis: A systematic review,” Aug. 14, 2019, *Institute of Physics Publishing*. doi: 10.1088/1741-2552/ab260c.

[130] J. W. Choi, S. Huh, and S. Jo, “Improving performance in motor imagery BCI-based control applications via virtually embodied feedback,” *Comput Biol Med*, vol. 127, Dec. 2020, doi: 10.1016/j.compbiomed.2020.104079.

[131] Y. Wang, X. Liu, H. Cui, Z. Li, and X. Chen, “An auditory selective attention brain-computer interface system based on auditory steady-state response,” *Applied Acoustics*, vol. 228, Jan. 2025, doi: 10.1016/j.apacoust.2024.110291.

[132] W. Zhang, A. Song, H. Hu, M. Miao, and B. Xu, “The application of vibration tactile stimulation in hand motor imagery paradigm: a pilot study,” *Brain-Apparatus Communication: A Journal of Bacomics*, vol. 3, no. 1, Dec. 2024, doi: 10.1080/27706710.2024.2383862.

[133] A. N. Mohammed, H. G. Alfughi, F. M. Alneqrat, H. A. Aghnaya, and A. A. Mohammed, “Utilising BCI Techniques for Controlling Robotic Arm Movements by Motor Imagery Signals,” in *2023 IEEE 11th International Conference on Systems and Control, ICSC 2023*, Institute of Electrical and Electronics Engineers Inc., 2023, pp. 899–904. doi: 10.1109/ICSC58660.2023.10449786.

[134] X. Y. Liu *et al.*, “Recent applications of EEG-based brain-computer-interface in the medical field,” Dec. 01, 2025, *BioMed Central Ltd*. doi: 10.1186/s40779-025-00598-z.

[135] M. Stone, “Cross-Validatory Choice and Assessment of Statistical Predictions,” 1974. [Online]. Available: https://about.jstor.org/terms

[136] V. Di Lazzaro *et al.*, “The effect on corticospinal volleys of reversing the direction of current induced in the motor cortex by transcranial magnetic stimulation,” *Exp Brain Res*, vol. 138, no. 2, pp. 268–273, 2001, doi: 10.1007/s002210100722.

[137] “Automatic 3D Intersubject Registration of MR Volumetric Data in Standardized Talairach Space”.

[138] L. Bonzano, A. Tacchino, L. Roccatagliata, G. Abbruzzese, G. L. Mancardi, and M. Bove, “Callosal contributions to simultaneous bimanual finger movements,” *Journal of Neuroscience*, vol. 28, no. 12, pp. 3227–3233, Mar. 2008, doi: 10.1523/JNEUROSCI.4076-07.2008.

[139] Y. J. Yang, E. J. Jeon, J. S. Kim, and C. K. Chung, “Characterization of kinesthetic motor imagery compared with visual motor imageries,” *Sci Rep*, vol. 11, no. 1, Dec. 2021, doi: 10.1038/s41598-021-82241-0.

[140] S. M. Christensen, N. S. Holm, and S. Puthusserypady, “An Improved Five Class MI Based BCI Scheme for Drone Control Using Filter Bank CSP.”

[141] Z. J. Kales, M. S. Lazar, and S. Z. Zhou, “Spatial Patterns Underlying Population Differences in the Background EEG,” 1990.

[142] C. R. J. del R. M. Iturrate I, *Handbook of Clinical Neurology, Chapter 23 - General principles of machine learning for brain-computer interfacing,* vol. 168. Elsevier, 2020.

[143] S. R. P. P. F. T. P M Rossini 1, “Corticospinal excitability modulation to hand muscles during movement imagery ,” *Cereb Cortex*, vol. 9, no. 2, pp. 161–167, 1999.

[144] V. Bruno, C. Fossataro, and F. Garbarini, “Inhibition or facilitation? Modulation of corticospinal excitability during motor imagery,” *Neuropsychologia*, vol. 111, no. September 2017, pp. 360–368, 2018, doi: 10.1016/j.neuropsychologia.2018.02.020.

[145] C. Neige, D. Rannaud Monany, C. M. Stinear, W. D. Byblow, C. Papaxanthis, and F. Lebon, “Unravelling the Modulation of Intracortical Inhibition During Motor Imagery: An Adaptive Threshold-Hunting Study,” *Neuroscience*, vol. 434, pp. 102–110, May 2020, doi: 10.1016/j.neuroscience.2020.03.038.

[146] S. Hétu *et al.*, “The neural network of motor imagery: An ALE meta-analysis,” Jun. 2013. doi: 10.1016/j.neubiorev.2013.03.017.

[147] N. Leeuwis, S. Yoon, and M. Alimardani, “Functional Connectivity Analysis in Motor-Imagery Brain Computer Interfaces,” *Front Hum Neurosci*, vol. 15, Oct. 2021, doi: 10.3389/fnhum.2021.732946.

[148] R. Aldea and M. Fira, “Classifications of Motor Imagery Tasks in Brain Computer Interface Using Linear Discriminant Analysis,” 2014. [Online]. Available: www.ijarai.thesai.org

[149] M. Arvaneh, C. Guan, K. K. Ang, and C. Quek, “Optimizing the channel selection and classification accuracy in EEG-based BCI,” *IEEE Trans Biomed Eng*, vol. 58, no. 6, pp. 1865–1873, Jun. 2011, doi: 10.1109/TBME.2011.2131142.